

Higgcision in the Two-Higgs Doublet Models

Kingman Cheung^{1,2}, Jae Sik Lee³, and Po-Yan Tseng¹

¹ *Department of Physics, National Tsing Hua University, Hsinchu 300, Taiwan*

² *Division of Quantum Phases and Devices, School of Physics,
Konkuk University, Seoul 143-701, Republic of Korea*

³ *Department of Physics, Chonnam National University,
300 Yongbong-dong, Buk-gu, Gwangju, 500-757, Republic of Korea*

(Dated: October, 2013)

Abstract

We perform global fits to general two-Higgs doublet models (2HDMs) with generalized couplings using the most updated data from ATLAS, CMS, and Tevatron. We include both scenarios with CP-conserving and CP-violating couplings. By relaxing the requirement on the discrete symmetries that are often imposed on the Yukawa couplings, we try to see which of the 2HDMs is preferred. We found that (i) Higgcision in 2HDMs can be performed efficiently by using only 4 parameters including the charged Higgs contributions to the Higgs couplings to two photons, (ii) the differences among various types of 2HDMs are very small with respect to the chi-square fits, (iii) $\tan\beta$ is constrained to be small, (iv) the p -values for various fits in 2HDMs are worse than that of the standard model. Finally, we put emphasis on our findings that future precision measurements of the Higgs coupling to the scalar top-quark bilinear (C_u^S) and $\tan\beta$ may endow us with the discriminating power among various types of 2HDMs especially when C_u^S deviates from its SM value 1.

I. INTRODUCTION

Upon the observation of a new boson at a mass around 125 GeV at the Large Hadron Collider (LHC) [1, 2], the Higgs precision (Higgcision) era has just begun. A study based on a generic framework for the deviations of the couplings from their standard model (SM) values shows [4] that the SM Higgs boson [3] provides the best fit to all the most updated Higgs data from ATLAS [5, 6], CMS [7–10], and Tevatron [11, 12].

In addition to a number of more or less model-independent studies [13–40], there are also studies done in the 2HDM [41–58] and supersymmetric [59–63] frameworks. In this work, we perform global fits to the general 2HDMs (*Higgcision in 2HDMs*) closely following the generic framework suggested in Ref. [4]. We use the most updated data from the ATLAS, CMS, and the Tevatron and include the scenarios with CP-conserving (CPC) and CP-violating (CPV) couplings. We find that Higgcision in 2HDMs can be performed very efficiently by using *only* 3 parameters (C_u^S , C_u^P , and $\tan\beta$, as shown later), if one can neglect the charged-Higgs contribution to the Higgs couplings to two photons. To consider the case when the charged-Higgs contribution to the $H\gamma\gamma$ couplings is significant, one may need only one additional parameter.

Furthermore, we relax the requirement on the discrete symmetries, which are often imposed on the Yukawa couplings to guarantee the absence of tree-level Flavor Changing Neutral Current (FCNC) [64], to see which of the 2HDMs is preferred. We find that the differences in the chi-squares among various types of 2HDMs are very small and one cannot see any preferences in both the CP-conserving and CP-violating cases.

A number of important findings in this work are:

1. the SM provides the best fit in terms of p -values. The general 2HDM fits at most improve marginally in the total χ^2 at the expense of additional parameters though, and so the p -values do not improve at all;
2. the differences among various types of 2HDMs are negligible in fitting the Higgs data;
3. the gauge boson coupling C_v is constrained to be close to 1, which means that the observed Higgs boson is responsible for the most part of the electroweak symmetry breaking; and
4. the $\tan\beta$ is constrained to a small value.

Finally, we emphasize that future precision measurements of C_u^S and $\tan\beta$ can provide us with the discriminating power among various types of 2HDMs especially when C_u^S deviates from its SM value 1.

The organization of the paper is as follows. In the next section, we describe the interactions of the Higgs bosons, including deviations in the Yukawa couplings and deviations in the loop functions of $H\gamma\gamma$, Hgg , and $HZ\gamma$ vertices, as well as the notation used in the analysis. In Sec. III, we fix the Higgs potential and Yukawa couplings of the general 2HDMs under consideration and describe how to perform Higgcision in 2HDMs. We articulate that only 4 fitting parameters are needed if we concentrate on the couplings of the candidate for the 125 GeV Higgs boson. We present the results of various fits in Sec. V and conclude in Sec. VI.

II. FORMALISM

For the Higgs couplings to the SM particles assuming the Higgs boson is a generic CP-mixed state without carrying any definite CP-parity, we follow the conventions and notations of CPsuperH [65–67] in which the Higgs couplings to fermions are given as

$$\mathcal{L}_{H\bar{f}f} = - \sum_{f=u,d,l} \frac{gm_f}{2M_W} H \bar{f} \left(g_{H\bar{f}f}^S + i g_{H\bar{f}f}^P \gamma_5 \right) f, \quad (1)$$

where $f = u, d, l$ stands for the up- and down-type quarks and charged leptons, respectively, and those to the massive vector bosons are

$$\mathcal{L}_{HVV} = g M_W \left(g_{HWW} W_\mu^+ W^{-\mu} + g_{HZZ} \frac{1}{2c_W^2} Z_\mu Z^\mu \right) H. \quad (2)$$

In the SM, $g_{H\bar{f}f}^S = 1$, $g_{H\bar{f}f}^P = 0$, and $g_{HWW} = g_{HZZ} \equiv g_{HVV} = 1$. For the loop-induced Higgs couplings to two photons, two gluons and $Z\gamma$, and their relevance to the couplings $g_{H\bar{f}f}^{S,P}$ and g_{HVV} , we refer to Refs. [4, 65–67]. Without loss of generality, we use the following notation for the parameters in the fits:

$$\begin{aligned} C_u^S &= g_{H\bar{u}u}^S, & C_d^S &= g_{H\bar{d}d}^S, & C_\ell^S &= g_{H\bar{\ell}\ell}^S; & C_v &= g_{HVV}; \\ C_u^P &= g_{H\bar{u}u}^P, & C_d^P &= g_{H\bar{d}d}^P, & C_\ell^P &= g_{H\bar{\ell}\ell}^P; \\ \Delta S^\gamma, & \Delta S^g, & \Delta P^\gamma, & \Delta P^g; \\ \Delta\Gamma_{\text{tot}}, & & & & & & & \end{aligned} \quad (3)$$

where ΔS^γ and ΔP^γ denote additional loop contributions to the loop factor S^γ and P^γ , respectively; and similarly for ΔS^g and ΔP^g . The $\Delta\Gamma_{\text{tot}}$ represents an additional nonstandard decay width of the Higgs boson (e.g., decay into the lighter Higgses). Here we assume generation independence and also custodial symmetry between the W and Z bosons.

Our analysis is based on the theoretical signal strength which may be approximated as the product

$$\hat{\mu}(\mathcal{P}, \mathcal{D}) \simeq \hat{\mu}(\mathcal{P}) \hat{\mu}(\mathcal{D}) \quad (4)$$

where $\mathcal{P} = \text{ggF}, \text{VBF}, \text{VH}, \text{ttH}$ denote the production mechanisms and $\mathcal{D} = \gamma\gamma, ZZ, WW, b\bar{b}, \tau\bar{\tau}$ the decay channels. For explicit expressions of $\hat{\mu}(\mathcal{P})$ and $\hat{\mu}(\mathcal{D})$, we again refer to Ref. [4], but by noting they are basically given by the ratios of the Higgs couplings to the corresponding SM ones.

III. 2HDMS

The general 2HDM potential may be given by [68]

$$\begin{aligned} V = & -\mu_1^2(\Phi_1^\dagger\Phi_1) - \mu_2^2(\Phi_2^\dagger\Phi_2) - m_{12}^2(\Phi_1^\dagger\Phi_2) - m_{12}^{*2}(\Phi_2^\dagger\Phi_1) \\ & + \lambda_1(\Phi_1^\dagger\Phi_1)^2 + \lambda_2(\Phi_2^\dagger\Phi_2)^2 + \lambda_3(\Phi_1^\dagger\Phi_1)(\Phi_2^\dagger\Phi_2) + \lambda_4(\Phi_1^\dagger\Phi_2)(\Phi_2^\dagger\Phi_1) \\ & + \frac{\lambda_5}{2}(\Phi_1^\dagger\Phi_2)^2 + \frac{\lambda_5^*}{2}(\Phi_2^\dagger\Phi_1)^2 + \lambda_6(\Phi_1^\dagger\Phi_1)(\Phi_1^\dagger\Phi_2) + \lambda_6^*(\Phi_1^\dagger\Phi_1)(\Phi_2^\dagger\Phi_1) \\ & + \lambda_7(\Phi_2^\dagger\Phi_2)(\Phi_1^\dagger\Phi_2) + \lambda_7^*(\Phi_2^\dagger\Phi_2)(\Phi_2^\dagger\Phi_1). \end{aligned} \quad (5)$$

With the parameterization

$$\Phi_1 = \begin{pmatrix} \phi_1^+ \\ \frac{1}{\sqrt{2}}(v_1 + \phi_1^0 + ia_1) \end{pmatrix}; \quad \Phi_2 = e^{i\xi} \begin{pmatrix} \phi_2^+ \\ \frac{1}{\sqrt{2}}(v_2 + \phi_2^0 + ia_2) \end{pmatrix} \quad (6)$$

and denoting $v_1 = v \cos \beta = v c_\beta$ and $v_2 = v \sin \beta = v s_\beta$, one may remove μ_1^2 , μ_2^2 , and $\Im m(m_{12}^2 e^{i\xi})$ from the 2HDM potential using three tadpole conditions. Then, including the vacuum expectation value v , one may need the following 13 parameters plus one sign:

$$\begin{aligned} & v, t_\beta, |m_{12}|; \\ & \lambda_1, \lambda_2, \lambda_3, \lambda_4, |\lambda_5|, |\lambda_6|, |\lambda_7|; \\ & \phi_5 + 2\xi, \phi_6 + \xi, \phi_7 + \xi, \text{sign}[\cos(\phi_{12} + \xi)]. \end{aligned} \quad (7)$$

to fully specify the general 2HDM potential. Here $m_{12}^2 = |m_{12}|^2 e^{i\phi_{12}}$ and $\lambda_{5,6,7} = |\lambda_{5,6,7}| e^{i\phi_{5,6,7}}$ and we note that $\sin(\phi_{12} + \xi)$ is fixed by the CP-odd tadpole condition when the CP phases

$\phi_5 + 2\xi$, $\phi_6 + \xi$ and $\phi_7 + \xi$ are given and, accordingly, $\cos(\phi_{12} + \xi)$ is determined up to the two-fold ambiguity. One may take the convention with $\xi = 0$ without loss of generality.

On the other hand, the Yukawa couplings are given in the interactions

$$\begin{aligned}
-\mathcal{L}_Y = & h_u \bar{u}_R Q^T (i\tau_2) \Phi_2 + h_d \bar{d}_R Q^T (i\tau_2) \left(-\eta_1^d \tilde{\Phi}_1 - \eta_2^d \tilde{\Phi}_2 \right) \\
& + h_l \bar{l}_R L^T (i\tau_2) \left(-\eta_1^l \tilde{\Phi}_1 - \eta_2^l \tilde{\Phi}_2 \right) + \text{h.c.}
\end{aligned} \tag{8}$$

where $Q^T = (u_L, d_L)$, $L^T = (\nu_L, l_L)$, and $\tilde{\Phi}_i = i\tau_2 \Phi_i^*$ with

$$i\tau_2 = \begin{pmatrix} 0 & 1 \\ -1 & 0 \end{pmatrix}. \tag{9}$$

We note that there is a freedom to redefine the two linear combinations of Φ_2 and Φ_1 to eliminate the coupling of the up-type quarks to Φ_1 [69]. The 2HDMs are classified according to the values of $\eta_{1,2}^l$ and $\eta_{1,2}^d$ as in Table I.

TABLE I. Classification of 2HDMs satisfying the Glashow-Weinberg condition [64] which guarantees the absence of tree-level FCNC.

	2HDM I	2HDM II	2HDM III	2HDM IV
η_1^d	0	1	0	1
η_2^d	1	0	1	0
η_1^l	0	1	1	0
η_2^l	1	0	0	1

By identifying the couplings

$$h_u = \frac{\sqrt{2}m_u}{v} \frac{1}{s_\beta}; \quad h_d = \frac{\sqrt{2}m_d}{v} \frac{1}{\eta_1^d c_\beta + \eta_2^d s_\beta}; \quad h_l = \frac{\sqrt{2}m_l}{v} \frac{1}{\eta_1^l c_\beta + \eta_2^l s_\beta}, \tag{10}$$

we have obtained the following Higgs-fermion-fermion interactions

$$\begin{aligned}
-\mathcal{L}_{H_i \bar{f} f} = & \frac{m_u}{v} \left[\bar{u} \left(\frac{O_{\phi_2 i}}{s_\beta} - i \frac{c_\beta}{s_\beta} O_{ai} \gamma_5 \right) u \right] H_i \\
& + \frac{m_d}{v} \left[\bar{d} \left(\frac{\eta_1^d O_{\phi_1 i} + \eta_2^d O_{\phi_2 i}}{\eta_1^d c_\beta + \eta_2^d s_\beta} - i \frac{\eta_1^d s_\beta - \eta_2^d c_\beta}{\eta_1^d c_\beta + \eta_2^d s_\beta} O_{ai} \gamma_5 \right) d \right] H_i \\
& + \frac{m_l}{v} \left[\bar{l} \left(\frac{\eta_1^l O_{\phi_1 i} + \eta_2^l O_{\phi_2 i}}{\eta_1^l c_\beta + \eta_2^l s_\beta} - i \frac{\eta_1^l s_\beta - \eta_2^l c_\beta}{\eta_1^l c_\beta + \eta_2^l s_\beta} O_{ai} \gamma_5 \right) l \right] H_i
\end{aligned} \tag{11}$$

and

$$\begin{aligned}
-\mathcal{L}_{H^\pm \bar{u}d} &= -\frac{\sqrt{2}m_u}{v} \left(\frac{c_\beta}{s_\beta} \right) \bar{u} P_L d H^+ - \frac{\sqrt{2}m_d}{v} \left(\frac{\eta_1^d s_\beta - \eta_2^d c_\beta}{\eta_1^d c_\beta + \eta_2^d s_\beta} \right) \bar{u} P_R d H^+ \\
&\quad - \frac{\sqrt{2}m_l}{v} \left(\frac{\eta_1^l s_\beta - \eta_2^l c_\beta}{\eta_1^l c_\beta + \eta_2^l s_\beta} \right) \bar{\nu} P_R l H^+ + \text{h.c.}
\end{aligned} \tag{12}$$

Here we take the convention with $\xi = 0$ and the couplings $h_{u,d,l}$ are supposed to be real. The 3×3 mixing matrix O is defined through

$$(\phi_1^0, \phi_2^0, a)_\alpha^T = O_{\alpha i} (H_1, H_2, H_3)_i^T \tag{13}$$

such that $O^T \mathcal{M}_0^2 O = \text{diag}(M_{H_1}^2, M_{H_2}^2, M_{H_3}^2)$ with the ordering of $M_{H_1} \leq M_{H_2} \leq M_{H_3}$. Here the 3×3 mass matrix of the neutral Higgs bosons \mathcal{M}_0^2 is given by

$$\mathcal{M}_0^2 = M_A^2 \begin{pmatrix} s_\beta^2 & -s_\beta c_\beta & 0 \\ -s_\beta c_\beta & c_\beta^2 & 0 \\ 0 & 0 & 1 \end{pmatrix} + \mathcal{M}_\lambda^2 \tag{14}$$

with (reinstating the relative phase ξ)

$$\begin{aligned}
M_A^2 &= M_{H^\pm}^2 + \frac{1}{2} \lambda_4 v^2 - \frac{1}{2} \Re(\lambda_5 e^{2i\xi}) v^2, \\
M_{H^\pm}^2 &= \frac{\Re(m_{12}^2 e^{i\xi})}{c_\beta s_\beta} - \frac{v^2}{2c_\beta s_\beta} \left[\lambda_4 c_\beta s_\beta + c_\beta s_\beta \Re(\lambda_5 e^{2i\xi}) + c_\beta^2 \Re(\lambda_6 e^{i\xi}) + s_\beta^2 \Re(\lambda_7 e^{i\xi}) \right],
\end{aligned} \tag{15}$$

and

$$\frac{\mathcal{M}_\lambda^2}{v^2} = \begin{pmatrix} 2\lambda_1 c_\beta^2 + \Re(\lambda_5 e^{2i\xi}) s_\beta^2 & \lambda_{34} c_\beta s_\beta + \Re(\lambda_6 e^{i\xi}) c_\beta^2 & -\frac{1}{2} \Im(\lambda_5 e^{2i\xi}) s_\beta \\ +2\Re(\lambda_6 e^{i\xi}) s_\beta c_\beta & +\Re(\lambda_7 e^{i\xi}) s_\beta^2 & -\Im(\lambda_6 e^{i\xi}) c_\beta \\ \lambda_{34} c_\beta s_\beta + \Re(\lambda_6 e^{i\xi}) c_\beta^2 & 2\lambda_2 s_\beta^2 + \Re(\lambda_5 e^{2i\xi}) c_\beta^2 & -\frac{1}{2} \Im(\lambda_5 e^{2i\xi}) c_\beta \\ +\Re(\lambda_7 e^{i\xi}) s_\beta^2 & +2\Re(\lambda_7 e^{i\xi}) s_\beta c_\beta & -\Im(\lambda_7 e^{i\xi}) s_\beta \\ -\frac{1}{2} \Im(\lambda_5 e^{2i\xi}) s_\beta & -\frac{1}{2} \Im(\lambda_5 e^{2i\xi}) c_\beta & 0 \\ -\Im(\lambda_6 e^{i\xi}) c_\beta & -\Im(\lambda_6 e^{i\xi}) s_\beta & \end{pmatrix} \tag{16}$$

where $\lambda_{34} = \lambda_3 + \lambda_4$ and, in passing, we note $v = gM_W/2$, $a = -s_\beta a_1 + c_\beta a_2$ and $H^+ = -s_\beta \phi_1^+ + c_\beta \phi_2^+$. We need to specify, therefore, the 13 parameters plus one sign listed in Eq. (7) to fix all the Higgs-fermion-fermion couplings.

Nevertheless, in order to calculate the signal strengths on which our chi-square analysis is based, we need to know only the couplings of the 125 GeV Higgs boson. Regarding the i -th Higgs boson H_i as the candidate for the 125 GeV Higgs boson, and by looking into Eqs. (11)

and (12), the relevant Higgs couplings can be fully determined by knowing the components $O_{\phi_1 i}$, $O_{\phi_2 i}$, and O_{ai} of the mixing matrix and t_β in each 2HDM. Comparing Eqs. (11) and (1) we find

$$\begin{aligned} O_{\phi_2 i} &= s_\beta C_u^S, \quad O_{ai} = -t_\beta C_u^P; \\ O_{\phi_1 i} &= \pm \left[1 - s_\beta^2 (C_u^S)^2 - t_\beta^2 (C_u^P)^2 \right]^{1/2}, \end{aligned} \quad (17)$$

where $C_u^S = g_{H_i \bar{u} u}^S$ and $C_u^P = g_{H_i \bar{u} u}^P$ and the orthogonality relation $(O_{\phi_1 i})^2 + (O_{\phi_2 i})^2 + (O_{ai})^2 = 1$ is used¹. Therefore, by specifying only the 3 parameters of C_u^S , C_u^P , and t_β , the couplings of the 125 GeV Higgs to all the SM fermions can be determined in each 2HDM as summarized in Table II. In addition, the Higgs coupling to the massive vector bosons is determined by

$$C_v = c_\beta O_{\phi_1 i} + s_\beta O_{\phi_2 i} = \pm c_\beta \left[1 - s_\beta^2 (C_u^S)^2 - t_\beta^2 (C_u^P)^2 \right]^{1/2} + s_\beta^2 C_u^S. \quad (18)$$

TABLE II. The couplings $C_{d,l}^{S,P}$ as functions of $C_u^{S,P}$ and $\tan \beta$ in each 2HDM.

2HDM I	$C_d^S = C_u^S$	$C_l^S = C_u^S$	$C_d^P = -C_u^P$	$C_l^P = -C_u^P$
2HDM II	$C_d^S = \pm \frac{[1 - s_\beta^2 (C_u^S)^2 - t_\beta^2 (C_u^P)^2]^{1/2}}{c_\beta}$	$C_l^S = \pm \frac{[1 - s_\beta^2 (C_u^S)^2 - t_\beta^2 (C_u^P)^2]^{1/2}}{c_\beta}$	$C_d^P = t_\beta^2 C_u^P$	$C_l^P = t_\beta^2 C_u^P$
2HDM III	$C_d^S = C_u^S$	$C_l^S = \pm \frac{[1 - s_\beta^2 (C_u^S)^2 - t_\beta^2 (C_u^P)^2]^{1/2}}{c_\beta}$	$C_d^P = -C_u^P$	$C_l^P = t_\beta^2 C_u^P$
2HDM IV	$C_d^S = \pm \frac{[1 - s_\beta^2 (C_u^S)^2 - t_\beta^2 (C_u^P)^2]^{1/2}}{c_\beta}$	$C_l^S = C_u^S$	$C_d^P = t_\beta^2 C_u^P$	$C_l^P = -C_u^P$

To recapitulate, we need 13 parameters (plus one sign) to fix all the Higgs couplings to the SM particles and the Higgs boson spectrum fully in general 2HDMs. In contrast, only 3 parameters are needed for the couplings of the 125 GeV Higgs candidate to the SM fermions and massive vector bosons. These 3 parameters are the two couplings of the 125 GeV Higgs candidate to the scalar and pseudoscalar top-quark bilinears (C_u^S and C_u^P , respectively) and $\tan \beta$. One may use C_v instead of $\tan \beta$ as shown later. In this work, we take advantage of the avenue with the smaller number of parameters to analyze the Higgs data.

With C_u^S , C_u^P , and C_v (or $\tan \beta$) given, we also need to know the charged Higgs contribution to the Higgs coupling to two photons in order to calculate the signal strengths. The

¹ Depending on the values of $\tan \beta$, C_u^S , and C_u^P , one may take one or both of the two signs for $O_{\phi_1 i}$ by fixing the relative sign between the Yukawa and $g_{H_i V V}$ couplings. Without loss of generality we take the convention of $g_{H_i V V} = C_v > 0$ in this work.

charged Higgs contribution to the Higgs coupling to two photons is given by

$$(\Delta S_i^\gamma)^{H^\pm} = -g_{H_i H^+ H^-} \frac{v^2}{2M_{H^\pm}^2} F_0(\tau_{iH^\pm}), \quad (19)$$

where $\tau_{iH^\pm} = M_{H_i}^2/4M_{H^\pm}^2$ and $F_0(\tau) = \tau^{-1} [-1 + \tau^{-1} f(\tau)]$ with

$$f(\tau) = -\frac{1}{2} \int_0^1 \frac{dy}{y} \ln [1 - 4\tau y(1-y)] = \begin{cases} \arcsin^2(\sqrt{\tau}) : & \tau \leq 1, \\ -\frac{1}{4} \left[\ln \left(\frac{\sqrt{\tau} + \sqrt{\tau-1}}{\sqrt{\tau} - \sqrt{\tau-1}} \right) - i\pi \right]^2 : & \tau \geq 1. \end{cases} \quad (20)$$

The $g_{H_i H^+ H^-}$ coupling is defined in the interaction

$$\mathcal{L}_{3H} = v \sum_{i=1}^3 g_{H_i H^+ H^-} H_i H^+ H^-, \quad (21)$$

with $g_{H_i H^+ H^-} = \sum_{\alpha=\phi_1, \phi_2, a} O_{\alpha i} g_{\alpha H^+ H^-}$. The effective couplings $g_{\alpha H^+ H^-}$ indeed involve all of the Higgs quartic couplings again and read [70]²:

$$\begin{aligned} g_{\phi_1 H^+ H^-} &= 2s_\beta^2 c_\beta \lambda_1 + c_\beta^3 \lambda_3 - s_\beta^2 c_\beta \lambda_4 - s_\beta^2 c_\beta \Re \lambda_5 + s_\beta (s_\beta^2 - 2c_\beta^2) \Re \lambda_6 \\ &\quad + s_\beta c_\beta^2 \Re \lambda_7, \\ g_{\phi_2 H^+ H^-} &= 2s_\beta c_\beta^2 \lambda_2 + s_\beta^3 \lambda_3 - s_\beta c_\beta^2 \lambda_4 - s_\beta c_\beta^2 \Re \lambda_5 + s_\beta^2 c_\beta \Re \lambda_6 \\ &\quad + c_\beta (c_\beta^2 - 2s_\beta^2) \Re \lambda_7, \\ g_{a H^+ H^-} &= s_\beta c_\beta \Im \lambda_5 - s_\beta^2 \Im \lambda_6 - c_\beta^2 \Im \lambda_7. \end{aligned} \quad (22)$$

Therefore, in order to include $(\Delta S_i^\gamma)^{H^\pm}$ one may specify all the quartic couplings and the charged Higgs mass in principle, but, then, the situation goes back to the original case with 13 parameters plus one sign. Nevertheless, even in this case one can still keep the spirit of efficiency and simplicity by treating $(\Delta S_i^\gamma)^{H^\pm}$ itself as another free parameter in addition to the other three ones C_u^S, C_u^P and C_v . And then, the results on $(\Delta S_i^\gamma)^{H^\pm}$ could be directly interpreted in terms of the coupling $g_{H_i H^+ H^-}$ of the 125 GeV Higgs boson to the charged Higgses and the charged Higgs boson mass M_{H^\pm} , as shown in Eq. (19).

One caveat of our approach to analyze the Higgs data with only 3 or 4 parameters is that one cannot say much about the other two neutral Higgs bosons and the charged one which, in principle, can be either heavier or lighter than the candidate for the 125 GeV Higgs. Before moving to the next section to present the results of various 2-, 3- and 4-parameter fits, we

² Note the convention difference for λ_5 by a factor 2.

would like to briefly comment on the status of experimental searches for the additional Higgs bosons.

At the LHC, both the ATLAS and CMS collaborations have searched for the additional neutral Higgs bosons up to 1 TeV through their decays into two massive vector bosons, $H_i \rightarrow ZZ$ or WW [71, 72]. Without observing any positive signal, they put an upper bound on the relevant cross section $\sigma(pp \rightarrow H_i \rightarrow VV)$ ³. The ATLAS collaboration performed the neutral Higgs-boson searches through the tau-lepton channel, $H_i \rightarrow \tau\tau$ [73]. While this applies for both the CP-even and CP-odd neutral Higgses up to 500 GeV, it was reported that the constraint for the additional CP-even Higgs from this channel is weaker than that from $H_i \rightarrow ZZ$ [74].

For the charged Higgs boson with mass around a few hundred GeV, the strongest constraint may come from $\text{BR}(\bar{B} \rightarrow X_s \gamma)$ through the additional loop contributions from the charged-Higgs bosons to the process $b \rightarrow s \gamma$ [74]. When the charged Higgs boson is lighter than the top quark, it can be searched at the LHC through the top-quark decay channel $t \rightarrow H^+ b$ with the charged Higgs boson subsequently decaying into $c\bar{b}$, $c\bar{s}$, and $\tau^+ \nu_\tau$. The direct searches of the charged Higgs boson at the LHC also set limits on the interactions of charged Higgs boson, but their constraints are still weaker than those from $\bar{B} \rightarrow X_s \gamma$ [74].

The current direct experimental searches for the additional Higgs bosons and their indirect effects on some flavor observables such as $\text{BR}(\bar{B} \rightarrow X_s \gamma)$ should provide more stringent restrictions on the model parameters in addition to those obtained by fitting the 125-GeV Higgs data only. This may deserve an independent study and we will discuss these crucial issues in detail in a future publication.

IV. FITS

As shown in the previous section, the whole analysis of the couplings of the observed Higgs boson (denoted by H_i) in 2HDMs, including the CP-conserving and CP-violating cases, can be performed with only 4 parameters: $C_u^S, C_u^P, C_v, (\Delta S_i^\gamma)^{H^\pm}$. In particular, we consider the following cases with respect to CP-conserving or CP-violating, and with/without charged Higgs contributions:

³ We note that, if CP is conserved, the constraints provided by these search channels cannot be applied to the CP-odd state.

- CP-conserving (CPC) cases
 - **CPC2**: C_u^S, C_v
 - **CPC3**: $C_u^S, C_v, (\Delta S^\gamma)^{H^\pm}$
- CP-violating (CPV) cases
 - **CPV3**: C_u^S, C_u^P, C_v
 - **CPV4**: $C_u^S, C_u^P, C_v, (\Delta S^\gamma)^{H^\pm}$

Here **CPC** and **CPV** represent CP-conserving and CP-violating fits, respectively, and the number denotes the number of varying parameters in each fit. In **CPC2** and **CPV3**, the charged Higgs contribution $(\Delta S^\gamma)^{H^\pm} = 0$. Note that the varying parameters should satisfy the following relations due to the unitarity of the mixing matrix:

$$s_\beta^2(C_u^S)^2 \leq 1, \quad t_\beta^2(C_u^P)^2 \leq 1, \quad s_\beta^2(C_u^S)^2 + t_\beta^2(C_u^P)^2 \leq 1. \quad (23)$$

One can use $\tan\beta$ in place of C_v in the analysis by exploiting the relation derived from Eq. (18):

$$s_\beta^2 = \frac{1 - C_v^2}{1 + (C_u^S)^2 + (C_u^P)^2 - 2C_v C_u^S}, \quad (24)$$

which is independent of sign $[O_{\phi_{1i}}]$. When $C_u^S = 1$ and $C_u^P = 0$, the above relation becomes $s_\beta^2 = (1 + C_v)/2$, which leads to $\tan\beta = \infty$ in the SM limit of $C_v = 1$. On the other hand, as in many models beyond the SM, if C_u^S and/or C_u^P deviate from its SM values 1 and 0, respectively, one may end up in the opposite limit, $\tan\beta = 0$, when the dynamics of the fit pushes C_v to its maximally allowed value or 1. In practice, one may wish to avoid the regions with small or (very) large $\tan\beta$ to maintain the perturbativity of the top and bottom Yukawa couplings h_t and h_b , respectively. We therefore restrict the range of $\tan\beta$ between 10^{-4} and 10^2 .

Before presenting our numerical results, we briefly review the current Higgs data. Current Higgs data focus on a few decay channels of the Higgs boson: (i) $h \rightarrow \gamma\gamma$, (ii) $h \rightarrow ZZ^* \rightarrow \ell^+\ell^-\ell^+\ell^-$, (iii) $h \rightarrow WW^* \rightarrow \ell^+\bar{\nu}\ell^-\nu$, (iv) $h \rightarrow b\bar{b}$, and (v) $h \rightarrow \tau^+\tau^-$. We have used 22 data points in our analysis as in Ref. [4]. To briefly summarize, the chi-square of all these 22 data points relative to the SM is

$$18.94 = 7.89(\gamma\gamma : 6) + 1.65(ZZ^* : 2) + 3.70(WW^* : 5) + 3.55(b\bar{b} : 4) + 2.15(\tau^+\tau^- : 5),$$

where the numbers in parentheses denote the number of data points in each decay mode. The chi-square per degree of freedom (dof) is about $18.94/22 = 0.86$ and the p -value is about $p_{\text{SM}} = 0.65$. We note the chi-square is dominated by the diphoton data with $\mu_{ggH+ttH}^{\text{ATLAS}} = 1.6 \pm 0.4$ and $\mu_{\text{untagged}}^{\text{CMS}} = 0.78_{-0.26}^{+0.28}$. Since the ATLAS data is about 1.5σ larger than the SM while the CMS one is about 1σ smaller, the dynamics of the fit cannot force the parameters to go into either direction.

A. CP conserving fits

In this subsection, we study the CP-conserving case with $C_u^P = 0$. In our numerical study, we find that $\tan\beta$ is bounded from above when C_u^S deviates from its SM value 1. Before presenting numerical results, we look into the correlation among the varying parameters C_u^S , C_v , and $\tan\beta$.

In the CP-conserving case, Eq. (18) simplifies into

$$C_v = \pm c_\beta \left[1 - s_\beta^2 (C_u^S)^2 \right]^{1/2} + s_\beta^2 C_u^S,$$

with the constraint $|s_\beta C_u^S| \leq 1$, which can be recast into the form

$$-\frac{1}{t_\beta} \leq C_u^S \leq \sqrt{1 + \frac{1}{t_\beta^2}}, \quad (25)$$

taking into account our convention of $C_v > 0$. For a given value of $\tan\beta$, we find that C_v takes the plus(+) sign as C_u^S increases from $-1/t_\beta$ (where $C_v = 0$) to $\sqrt{1 + 1/t_\beta^2}$. While it takes the minus(-) sign when C_u^S goes from the maximum value $\sqrt{1 + 1/t_\beta^2}$ back to $1/t_\beta$ where again $C_v = 0$. Therefore, C_v has two positive solutions if C_u^S lies between $1/t_\beta$ and $\sqrt{1 + 1/t_\beta^2}$. This behavior is shown in the left frame of Fig. 1. From Eq. (24) which now can be rearranged into the form

$$s_\beta^2 = \frac{(1 - C_v^2)}{(1 - C_v^2) + (C_u^S - C_v)^2},$$

we can see that $\sin\beta = 1$ or $\tan\beta = \infty$ along the line $C_v = C_u^S$. Also, the larger $\tan\beta$ the smaller C_v will be. Therefore, $\tan\beta$ will be bounded from above when C_v is pushed to be close to 1, unless $C_u^S = 1$.

To be more precise, we consider the situation in which C_v is constrained as $C_v > (C_v)_{\text{min}}$. As illustrated in the right frame of Fig. 1 with three values of $C_u^S = 0.9$ (black), 1 (red), and

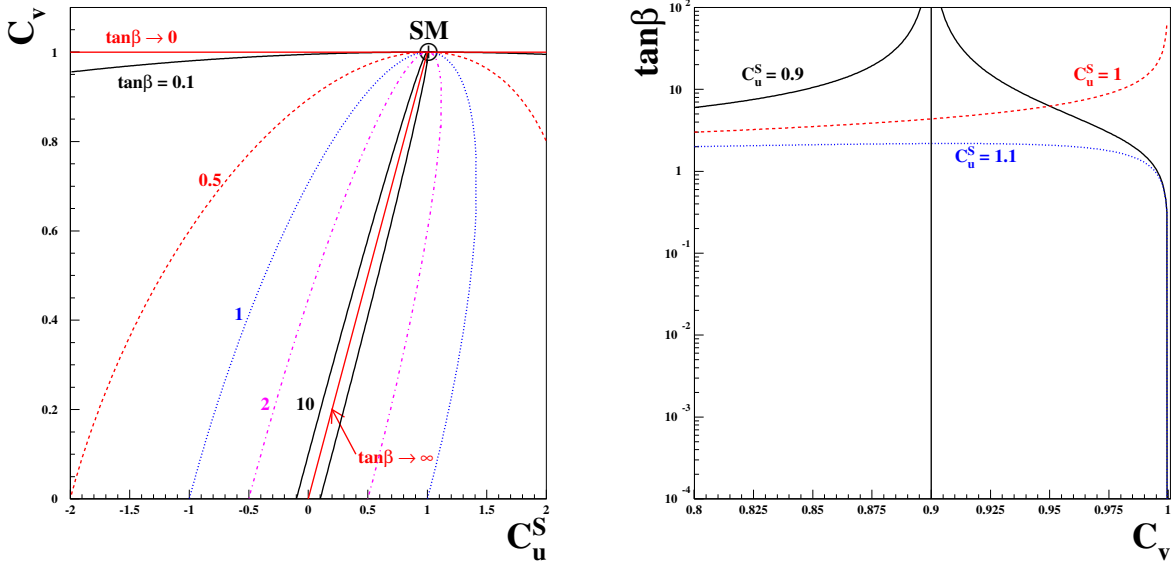


FIG. 1. (Left) C_v as functions of C_u^S for several values of $\tan\beta = 0.1$ (black) 0.5 (red), 1 (blue), 2 (magenta), and 10 (black). The horizontal red line is for the limit $\tan\beta \rightarrow 0$ and the straight red line with $C_v = C_u^S$ represents the limits $\tan\beta \rightarrow \infty$. The SM point with $C_v = C_u^S = 1$ is denoted by \oplus . (Right) $\tan\beta$ as functions C_v for three values of $C_u^S = 0.9$ (black), 1 (red), and 1.1 (blue). The vertical line shows the location $C_v = 0.9$.

1.1 (blue), we have found that $\tan\beta$ has an upper bound when $C_u^S < (C_v)_{\min}$ for $C_u^S < 1$. We observe that the upper bound on $\tan\beta$ is stronger when $(C_v)_{\min}$ is closer to 1 but it disappears when $(C_v)_{\min} < C_u^S$ or $C_u^S = 1$. On the other hand, when $C_u^S > 1$, $\tan\beta$ is always bounded by $\tan\beta \leq 1/\sqrt{(C_u^S)^2 - 1}$, see Eq. (25). Requiring $C_v > 0.95$, for example, we find $\tan\beta \lesssim 6$ for $C_u^S = 0.9$ and $\tan\beta \lesssim 1/\sqrt{(C_u^S)^2 - 1} \simeq 2$ for $C_u^S = 1.1$.

In the following sub-subsections, we illustrate that the precise and independent measurements of C_u^S and $\tan\beta$ can tell us the phenomenological viability of 2HDMs and/or enable us to make discrimination among them.

The results for various fits (**CPC2**, **CPC3**, **CPV3**, and **CPV4**) are tabulated in Tables III and IV, and confidence regions are shown in Figs. 2 – 21.

1. CPC2

The fit **CPC2** analyzes the Higgs data by varying C_u^S and C_v (or equivalently $\log_{10} \tan \beta$). The total χ^2 , χ^2/dof , p -value and the best-fit values of C_u^S , C_v , and $\tan \beta$ for the types I – IV of 2HDMs are shown at the top of Table III. We have found that the type-I model gives the smallest χ^2 but the variation of total χ^2 among the 4 types is very small, within 0.29. Statistically, there is no preference among any type I to IV of 2HDMs. We note that the p -values of the fits are all worse than the SM one $p_{\text{SM}} = 0.65$. The best-fit values for C_u^S are about 0.9 for type I and III, and about 0.96 for type II and IV. The fitted C_v 's are very close to the theoretically allowed maximum value 1 independent of the type. In the actual implementation, we used $\log_{10} \tan \beta$ as the scanning variable with $-4 < \log_{10} \tan \beta < 2$, instead of C_v . Again, independent of the type, χ^2 continues to decrease as $\tan \beta$ falls below its lower limit $\tan \beta = 10^{-4}$, though extremely slowly. The best fitted values for $\tan \beta$ are denoted by *limit* in Table III.

We show the contour plots for confidence-level regions as functions C_u^S vs C_v , C_u^S vs $\tan \beta$, and C_d^S vs C_l^S in Figs. 2 – 4, respectively. The regions shown are for $\Delta\chi^2 \leq 2.3$ (red), 5.99 (green), and 11.83 (blue) above the minimum, which correspond to confidence levels of 68.3%, 95%, and 99.7%, respectively. The best-fit point is denoted by the triangle. We note that from Fig. 2 there are two islands and positive C_u^S is preferred. At 99.7% confidence level (CL), $C_v \gtrsim 0.7$. We also find that C_u^S takes on the values between 0.71 and 1.2 (I), 0.86 and 1.1 (II), 0.71 and 1.2 (III), and 0.86 and 1.1 (IV) at 68.3 % CL. Comparing type I with the other three types, we find that the preference for $C_u^S = 1$ is stronger in type II, III, and IV, and C_v is more strongly constrained to be close to 1 unless $C_u^S = 1$. Furthermore, the $\tan \beta = \infty$ line with $C_u^S = C_v$ passes through the CL regions only in type I.

In Fig. 3, we show the CL regions in the plane of C_u^S and $\tan \beta$. For $\tan \beta \lesssim 0.5$, we find χ^2 is almost independent of $\tan \beta$ for a fixed value of C_u^S ; while for $\tan \beta \gtrsim 1$, the values of C_u^S is constrained by $C_u^S \leq \sqrt{1 + 1/t_\beta^2}$. For type I, as we observed in Fig. 2, the $\tan \beta = \infty$ line passes through the CL regions and it explains why we can have very large $\tan \beta$ in relatively broader range of C_u^S . For the other three types it is only possible to have very large $\tan \beta$ in the narrow region around $C_u^S = 1$. Thus, in these cases we find that $\tan \beta \lesssim 3$ (II), 2 (III), 3 (IV) at 99.7 % CL when the best-fit value of C_u^S is taken in each of the type II, III, and IV. If precise and independent measurements of C_u^S and $\tan \beta$ are available in

future experiments, one can tell the phenomenological viability of 2HDMs. For example, if $\tan\beta \gtrsim 10$ and $C_u^S \neq 1$, then one can rule out the type II, III, and IV models based on Fig. 3.

In Fig. 4, we show the CL regions in the plane of C_d^S and C_l^S . From Table II, the following relations $C_d^S = C_l^S = C_u^S$ (I), $C_d^S = C_l^S$ (II), $C_d^S = C_u^S$ (III), and $C_l^S = C_u^S$ (IV) are hold. In Table IV, we can see that the best-fit values of C_d^S and/or C_l^S are +1 unless either or both of them are equal to C_u^S . This can be understood from the relation, for example in type II,

$$C_d^S = C_l^S = \frac{\sqrt{1 - s_\beta^2 (C_u^S)^2}}{c_\beta} = \sqrt{1 + t_\beta^2 [1 - (C_u^S)^2]} \quad (26)$$

with the best-fit values of $C_u^S = 0.963$ and $\tan\beta = \text{limit} = 10^{-4}$. Note that the positive sign is selected to explain the best-fit values of $C_{d,l}^S$. Taking into account the negative sign, we observe that the points around $(C_d^S, C_l^S) = (-1, -1)$ (II), $(C_d^S, C_l^S) = (+1, -1)$ (III), and $(C_d^S, C_l^S) = (-1, +1)$ (IV) are also allowed at 68.3 % CL even when C_u^S is positive.

So far in this **CPC2** fit we only found very small χ^2 differences among the four types. What if the discrete symmetries are relaxed, do we get a better χ^2 fit? We relax the requirement on the discrete symmetries, which enforces $\eta_{1,2}^{d,\ell}$ to be either 0 or 1, but still require $(\eta_1^{d,\ell})^2 + (\eta_2^{d,\ell})^2 = 1$. We therefore have two more free parameters in our scan, and they are $\eta_1^{d,\ell}$, leading to a four-parameter fit by varying C_u^S , C_v , η_1^d , and η_1^ℓ . In Fig. 5, we show the CL regions of the fit by varying C_u^S , C_v , η_1^d , and η_1^ℓ in the plane of η_1^d and η_1^ℓ ⁴. We observe that $\Delta\chi^2 < 1$ in the whole (η_1^d, η_1^ℓ) plane, and so conclude that one cannot say any preference based on the current Higgs data.

2. **CPC3**

In this **CPC3** fit, we vary three parameters: C_u^S , C_v (or equivalently $\log_{10} \tan\beta$), and $(\Delta S^\gamma)^{H^\pm}$. The total χ^2 , χ^2/dof , p -value and the best-fit values of C_u^S , C_v ($\tan\beta$), and $(\Delta S^\gamma)^{H^\pm}$ for the types I – IV of 2HDMs are shown in the upper half of Table III. We show the contour plots for confidence-level regions as functions C_u^S vs C_v , C_u^S vs $\tan\beta$, C_u^S vs $(\Delta S^\gamma)^{H^\pm}$, and C_d^S vs C_l^S in Figs. 6 – 9, respectively.

We found that type II gives the smallest χ^2 but the variation of total χ^2 among the four types is very small, within 0.34. The **CPC3** fit is slightly better than the **CPC2**, as it has

⁴ We obtain the minimum $\chi^2 = 18.30$ and $\chi^2/\text{dof} = 1.02$ for this fit.

one more parameter in the fit. However, the p -values of the fits are still worse than the SM one ($p_{\text{SM}} = 0.65$). The best-fit values for C_u^S are about ± 0.92 (I), -0.82 (II), -0.91 (III), and 0.96 (IV) and those of C_v are 0.97 for I and III and 1 for II and IV. We also implement independent fits with $\log_{10} \tan \beta$ as the scanning variable taking $-4 < \log_{10} \tan \beta < 2$, instead of C_v . The best-fit values for $\tan \beta$ are either small or very small, except for type I with positive C_u^S . Again, we note that χ^2 hardly changes as $\tan \beta$ varies in wide range of parameter space.

For $(\Delta S^\gamma)^{H^\pm}$, we have obtained $(\Delta S^\gamma)^{H^\pm} \simeq -0.8$ or 2.3 when $C_u^S \sim +0.9$ or -0.9 , respectively. This can be understood from the numerical expression for S^γ [4]

$$S^\gamma \simeq -8.35 C_v + 1.76 C_u^S + (\Delta S^\gamma)^{H^\pm}. \quad (27)$$

When C_u^S changes from $+0.9$ to -0.9 , $(\Delta S^\gamma)^{H^\pm}$ changes from -0.8 to $+2.3$ so that the sum $1.76 C_u^S + (\Delta S^\gamma)^{H^\pm} \approx 0.7$.

The contour plots for the CL regions in the plane of C_u^S vs C_v for type I – IV are shown in Fig. 6, which can be directly compared to Fig. 2. In contrast, the negative C_u^S is now equally as good as the positive one. We show the CL regions in the plane of C_u^S and $\tan \beta$ in Fig. 7. For the negative C_u^S case, we find that $\tan \beta$ is smaller than ~ 0.6 at 99.7 % CL. In Fig. 8, we show the CL regions in the plane of C_u^S and $(\Delta S^\gamma)^{H^\pm}$. For positive C_u^S , it lies between 2 and -4 while $(\Delta S^\gamma)^{H^\pm} > -0.7 \sim -1.6$ for negative C_u^S at 99.7 % CL. The CL regions for C_l^S and C_d^S are similar to the **CPC2** case as shown in Fig. 9 but with the larger regions allowed at 68.5 % CL around the negative values of couplings.

The single parameter $(\Delta S^\gamma)^{H^\pm}$ can be interpreted in terms of the charged Higgs mass M_{H^\pm} and the neutral Higgs coupling to the charged Higgses $g_{H_i H^+ H^-}$, as in Eq. (19). In Fig. 10, we show the CL regions in the plane of M_{H^\pm} vs $g_{H_i H^+ H^-}$. Since the variation of χ^2 is very mild, we add one more region with $\Delta\chi^2 \leq 1$ (black). The thick cyan lines denote the points giving the best-fit values of $(\Delta S^\gamma)^{H^\pm}$ in each type given by Eq. (19). We see that a smaller charged Higgs mass is preferred when $g_{H_i H^+ H^-} < 0$, because this corresponds to $C_u^S < 0$ and so a larger $(\Delta S^\gamma)^{H^\pm} \approx 2.3$ is required. If the charged Higgs mass is larger than ~ 300 GeV as in the type II model constrained by $B(b \rightarrow s\gamma)$, we can see that the positive C_u^S case with $(\Delta S^\gamma)^{H^\pm} \sim -0.8$ is somewhat preferred. Nevertheless, the variation of χ^2 is not large enough to have a conclusive statement based on the current Higgs data.

B. CP violating fits

In this subsection, we study the CP-violating case with a nonzero C_u^P in addition to C_u^S , C_v (or, equivalently, $\tan\beta$), and $(\Delta S\gamma)^{H^\pm}$. In our numerical study, we again find that $\tan\beta$ is bounded from above when C_u^S deviates from its SM value 1. So, as in the CP-conserving case, the precise and independent future measurements of C_u^S and $\tan\beta$ can tell us the phenomenological viability of 2HDMs, thus providing some possible model discriminating power.

1. CPV3

In the **CPV3** fit, we vary C_u^S , C_u^P , and C_v (or equivalently $\log_{10}\tan\beta$). The other couplings $C_{d,l}^{S,P}$ are given by the relations shown in Table II. The total χ^2 , χ^2/dof , p -value, and the best-fit values for C_u^S , C_u^P , and C_v ($\tan\beta$) for the types I – IV 2HDMs are shown in the lower half of Table III. We show the contour plots for confidence-level regions as functions C_u^S vs C_u^P , C_u^S vs C_v , C_u^S vs $\tan\beta$, C_d^S vs C_d^P , and C_l^S vs C_l^P in Figs. 11 – 15, respectively. We found that type II gives the smallest χ^2 and the variation of total χ^2 among the 4 types is within 1.2, which is about 4 times larger compared to the CP-conserving case. Yet, such small χ^2 differences cannot help us to preferentially select one of the types. The best p -value for type II is 0.578, which is the largest among all the fits considered in this work, but it is still smaller than the SM $p_{\text{SM}} = 0.65$.

The best-fit values for C_u^S are all positive: 0.87 (I), 0.48 (II), 0.87 (III) and 0.81 (IV); while we have both the positive and negative best-fit values for C_u^P : ± 0.15 (I), ± 0.51 (II), ± 0.11 (III) and ± 0.34 (IV). Note that the largest (almost maximal) CP violation can occur in type II with $C_u^S \sim |C_u^P| \sim 0.5$. The best-fit values for C_v are 0.99 (I) and 1 (II, III and IV), and those for $\tan\beta$ are 0.9 (I), 0.1 (II), and $\sim 10^{-4}$ (III and IV).

The CL regions in the C_u^S and C_u^P plane are shown in Fig. 11. A positive C_u^S is in general preferred and it takes a value between 0.44 and 1.1 (I), -0.30 and 1.1 (II), 0.64 and 1.2 (III), and 0.26 and 1.1 (IV) at 68.3 % CL. For C_u^P , the 68.3 % CL regions are between: -0.55 and $+0.55$ (I), -0.70 and $+0.70$ (II), -0.45 and $+0.45$ (III), and -0.73 and $+0.73$ (IV). We note that maximal CP violation with $C_u^S \sim |C_u^P|$ is possible even when $C_v \simeq 1$. This can be

understood by considering the relation Eq. (18), which takes on a form of

$$C_v = 1 - \frac{1}{2}\beta^2 \left[(C_u^S - 1)^2 + (C_u^P)^2 \right] + \mathcal{O}(\beta^3) \quad (28)$$

in the $\tan \beta = 0$ limit. Taking an example of $C_u^S = C_u^P = 1/2$, one may have

$$O_{\phi_2 i} = \beta/2, \quad O_{ai} = -\beta/2, \quad O_{\phi_1 i} = 1 - \beta^2/4, \quad C_v = 1 - \beta^2/4 \quad (29)$$

up to $\mathcal{O}(\beta^3)$. Hence, although the 126-GeV observed state is mostly CP-even dominated by the ϕ_1 component, it can have maximally CP-violating couplings to the up-type quarks with $C_u^S = |C_u^P| = 1/2$.

In Figs. 12 and 13, we show the CL regions in the C_u^S vs C_v and C_u^S vs $\tan \beta$ planes, respectively. Compared to the CPC case, we observe that the two islands are now merged together, except for type III. We again find that $\tan \beta$ is bounded from above: $\tan \beta \lesssim 1$ (II), $\tan \beta \lesssim 3$ (III), and $\tan \beta \lesssim 2$ (IV). As in the CPC case, considerable deviation of C_u^S from 1 for large $\tan \beta \gtrsim 10$ is not possible in the type II, III, IV models.

In Fig. 14, we show the Higgs couplings to the down-type quarks. The behavior can be understood by observing the relations $C_d^S = C_u^S$ and $C_d^P = -C_u^P$ (I and III) and $C_d^S = \pm \left\{ 1 + t_\beta^2 [1 - (C_u^S)^2] - t_\beta^4 / s_\beta^2 (C_u^P)^2 \right\}^{1/2}$ and $C_d^P = t_\beta^2 C_u^P$ (II and IV), see Table II. Note that $|C_d^P| \lesssim 1$ at 99.7 % CL. We observe large CP violation is possible in the Higgs couplings to the down-type quarks.

In Fig. 15, we show the Higgs couplings to the charged leptons. Now the couplings are given by $C_l^S = C_u^S$ and $C_l^P = -C_u^P$ (I and IV) and $C_l^S = \pm \left\{ 1 + t_\beta^2 [1 - (C_u^S)^2] - t_\beta^4 / s_\beta^2 (C_u^P)^2 \right\}^{1/2}$ and $C_l^P = t_\beta^2 C_u^P$ (II and III). Again we note that $|C_l^P| \lesssim 1$ at 99.7 % CL and large CP violation is also possible in the Higgs couplings to the charged leptons.

Before we close this sub-subsection, we make a comment on the figures for the CL regions in the planes of C_d^S vs C_d^P and C_l^S vs C_l^P . Unless $(C_{d,l}^S, C_{d,l}^P) = (C_u^S, -C_u^P)$, the boundaries of the CL regions are somewhat fuzzy as shown in the frames for type II and IV of Fig. 14 and in those for type II and III of Fig. 15. We figure out that this is because one has $(C_{d,l}^S, C_{d,l}^P) \sim (1, 0)$ in most of the parameters space due to the coupling relations shown in Table II. Furthermore, we have the fewer points on the negative side of C_d^S or C_l^S . For the couplings $C_{d,l}^S$ to be negative, the negative sign needs to be chosen for $O_{\phi_1 i}$ in Eq. (17). But we note that the other positive sign is chosen mostly for $O_{\phi_1 i}$ due to the choice of $C_v > 0$ made in the analysis. Similar behavior happens in Fig. 20 and Fig. 21.

2. CPV4

In the **CPV4** fit, we vary C_u^S , C_u^P , C_v (or $\log_{10} \tan \beta$ equivalently), and $(\Delta S\gamma)^{H^\pm}$. The other couplings $C_{d,l}^{S;P}$ are given by the relations shown in Table II. The total χ^2 , χ^2/dof , p -value and the best-fit values for C_u^S , C_u^P , C_v ($\tan \beta$), and $(\Delta S\gamma)^{H^\pm}$ for the four types of 2HDMs can be found in the lower half of Table III. We show the contour plots for confidence-level regions as functions C_u^S vs C_u^P , C_u^S vs C_v , C_u^S vs $\tan \beta$, C_u^S vs $(\Delta S\gamma)^{H^\pm}$, C_d^S vs C_d^P , and C_l^S vs C_l^P in Figs. 16 – 21, respectively. We find that type II gives the smallest χ^2 and its variation among the 4 types is within 0.57, which is smaller than that of the **CPV3** fits. The p -values of the **CPV4** fits are also worse than the **CPV3** fits.

The best-fit values for C_u^S are about ± 0.92 (I), -0.05 (II), -0.91 (III) and 0.96 (IV), while those of C_u^P are about 0 (I), ± 0.57 (II), 0.03 (III), and -0.02 (IV). In type II, we note the best-fit value for C_u^S is almost 0 and those of C_u^P are very small except for type II. Therefore, in terms of the best-fit values the measure of CP-violating effect $2C_u^S C_u^P / [(C_u^S)^2 + (C_u^P)^2]$ is not significant in all 4 types of 2HDMs. Nevertheless, the CP violation could be significant taking account of the errors. For the Higgs couplings to the down-type quarks and charged leptons, we find that all the couplings C_d^P and C_l^P are almost vanishing: see Table IV. The best-fit values for C_v are about 0.97 (I and III) and 1 (II and IV) and those for $\tan \beta$ are $\mathcal{O}(0.1)$, except for type I with positive C_u^S , where the best-fit value is 6.5. As will be shown below in the figures, variation of χ^2 vs of $\tan \beta$ is small in a large region of parameter space. For $(\Delta S\gamma)^{H^\pm}$, the best-fit values are -0.78 and 2.4 (I), 1.0 (II), 2.4 (III), and -0.83 (IV). This also can be understood from Eq. (27).

In Fig. 16, we show the CL regions in the C_u^S and C_u^P plane, and note that the positive and negative C_u^S regions are providing equally good fits. The 68 % CL regions of C_u^S are: $-1.1 \sim -0.5$ and $0.5 \sim 1.1$ (I), $-1 \sim 1$ (II), $-1.2 \sim -0.5$ and $0.6 \sim 1.2$ (III), and $-1 \sim -0.4$ and $0.3 \sim 1.1$ (IV). Also, C_u^P varies between ± 0.5 (I, III) and ± 0.7 (II, IV) in the 68 % CL regions. Therefore, the maximal CP violation with $|C_u^S| = |C_u^P|$ is still possible.

We show the CL regions in the C_u^S - C_v and C_u^S - $\tan \beta$ planes in Figs. 17 and 18, respectively. $C_v \gtrsim 0.8$ at 68 % CL and $\tan \beta$ are bounded from above for the type II, III, and IV, except for a narrow region around $C_u^S = 1$. The CL regions in the plane of C_u^S and $(\Delta S\gamma)^{H^\pm}$ are shown in Fig. 19. Roughly speaking, $-2 \lesssim (\Delta S\gamma)^{H^\pm} \lesssim 3.5$ (68 % CL). In Figs. 20 and 21, the Higgs couplings to the down-type quarks and charged leptons are shown.

Finally, the single parameter $(\Delta S^\gamma)^{H^\pm}$ can be interpreted in terms of the charged Higgs mass M_{H^\pm} and the neutral Higgs coupling to the charged Higgses $g_{H_i H^+ H^-}$, as in Eq. (19). In Fig. 22, we show the CL regions in the plane of M_{H^\pm} vs $g_{H_i H^+ H^-}$. Compared to the **CPC3** case, we have $\Delta\chi^2 \leq 1$ in the wider range.

V. DISCUSSION

In this work, we have applied our previous model-independent approach [4], which analyzes all the observed Higgs boson signal strengths and fits to all the Higgs boson couplings, to the 2HDMs. In 2HDMs, the Higgs couplings to up-type and down-type quarks, and charged leptons are related by a set of relations shown in Table II. We have shown that the whole analysis can be performed with at most 3 independent parameters: C_u^S , C_v (or $\tan\beta$), and $(\Delta S^\gamma)^{H^\pm}$ for CP-conserving scenarios, and only one more parameter C_u^P for the CP-violating scenarios. A number of relationships among the couplings of the up- and down-type quarks and charged leptons have been derived such that we need only C_u^S and C_u^P .

A set of discrete symmetries are often imposed in literature in order to eliminate flavor-changing neutral currents, denoted by the parameters $\eta_{1,2}^{d,l}$, which take up the values either 0 or 1. The four combinations of $(\eta_1^d, \eta_1^l) = (0, 0), (1, 1), (0, 1), (1, 0)$ correspond to type I, II, III, and IV, respectively. We have demonstrated that the current Higgs boson data have no preference for any of the four types of 2HDMs, because statistically the χ^2 difference among type I–IV is only 0.3 for CPC cases and 1.2 for CPV cases: see Table III. We also relaxed the discrete symmetries to allow continuous values for $\eta_{1,2}^{d,l}$ subject to normalization $(\eta_1^{d,l})^2 + (\eta_2^{d,l})^2 = 1$, and we found that in the whole plane of $0 \leq \eta_1^d, \eta_1^l \leq 1$ the χ^2 differences among the best-fits are all within $\chi^2 < 1.2$. It is one of the main findings in this work – no particular preference among type I to IV as long as the current Higgs boson data are concerned.

The Higgs data used are almost the final set out of the 7 TeV and 8 TeV runs at the LHC. Further improvement to the fits will only be possible when more data are pouring in the next run of 2015. So far, the data have pointed to the SM Higgs boson with a large p -value, while all other extensions to the SM, such as the 2HDMs studied in this work or more model-independently in Ref. [4], provide fits with smaller p -values than the SM. It

means that the SM Higgs boson is currently the best explanation to all the Higgs boson data.

We offer a few more comments before we conclude.

1. The up-type and down-type (charged lepton) Yukawa couplings are related by quark masses and $\tan \beta$. Therefore, one set of parameters C_u^S , C_u^P , and $\tan \beta$ is sufficient to define all the fermionic couplings.
2. When we relax the discrete symmetries by varying η_1^d and η_1^l , we found the best-fit values for them are neither 0 nor 1. However, the χ^2 differences in the whole plane of η_1^d vs η_1^l are too small to claim any preference statistically.
3. The charged Higgs boson contributes to the one-loop vertex $H\gamma\gamma$. In the studies, we first treated $(\Delta S\gamma)^{H^\pm}$ as an independent parameter. Then we broke it down into the charged Higgs mass M_{H^\pm} and the coupling $g_{H_i H^+ H^-}$. When the $b \rightarrow s\gamma$ constraint (roughly $M_{H^\pm} > 300$ GeV) is taken into account, positive $g_{H_i H^+ H^-}$ is preferred.
4. The Higgs coupling to gauge bosons C_v is constrained to be very close to 1. It means that the observed Higgs boson is entirely responsible for breaking the electroweak symmetry.
5. Future precision measurements of C_u^S and $\tan \beta$ can provide us with the discriminating power among various types of 2HDMs especially when C_u^S deviates from its SM value 1.
6. The parameters C_u^S and C_u^P are constrained in the form of some ellipses. The current Higgs observables are not sensitive to CP-violating effects, and so only combinations of scalar and pseudoscalar Yukawa couplings are constrained, as shown in Figs. 11 and 16.
7. Among the 2HDM fits considered in this work, the type-II CP-violating case with $(\Delta S\gamma)^{H^\pm} = 0$ (the **CPV3** type-II fit) gives the best fit with $\chi^2 = 17.17$ and p -value = 0.578 when $C_u^S \sim |C_u^P| = 1/2$.

ACKNOWLEDGMENT

This work was supported the National Science Council of Taiwan under Grants No. 99-2112-M-007-005-MY3 and 102-2112-M-007-015-MY3. J.S.L. was supported by the National Research Foundation of Korea (NRF) grant (No. 2013R1A2A2A01015406). This study was also financially supported by Chonnam National University, 2012.

-
- [1] G. Aad *et al.* [ATLAS Collaboration], Phys. Lett. B **716**, 1 (2012) [arXiv:1207.7214 [hep-ex]].
 - [2] S. Chatrchyan *et al.* [CMS Collaboration], Phys. Lett. B **716**, 30 (2012) [arXiv:1207.7235 [hep-ex]].
 - [3] P. W. Higgs, Phys. Rev. Lett. **13**, 508 (1964); F. Englert and R. Brout, Phys. Rev. Lett. **13**, 321 (1964); G. S. Guralnik, C. R. Hagen and T. W. B. Kibble, Phys. Rev. Lett. **13**, 585 (1964).
 - [4] K. Cheung, J. S. Lee and P. -Y. Tseng, “Higgs Precision (Higgcision) Era begins,” JHEP **1305** (2013) 134 [arXiv:1302.3794 [hep-ph]].
 - [5] The ATLAS Collaboration, ATLAS-CONF-2013-012, “Measurements of the properties of the Higgs-like boson in the two photon decay channel with the ATLAS detector using 25 fb⁻¹ of proton-proton collision data” (Mar. 2013).
 - [6] The ATLAS Collaboration, ATLAS-CONF-2013-034, “Combined coupling measurements of the Higgs-like boson with the ATLAS detector using up to 25 fb⁻¹ of proton-proton collision data” (Mar. 2013).
 - [7] The CMS Collaboration, CMS PAS HIG-13-001, “Updated measurements of the Higgs boson at 125 GeV in the two photon decay channel” (Mar. 2013).
 - [8] The CMS Collaboration, CMS PAS HIG-13-002, “Properties of the Higgs-like boson in the decay $H \rightarrow ZZ \rightarrow 4l$ in pp collisions at $\sqrt{s} = 7$ and 8 TeV” (Mar. 2013).
 - [9] The CMS Collaboration, CMS PAS HIG-13-003, “Update on the search for the standard model Higgs boson in pp collisions at the LHC decaying to W^+W^- in the fully leptonic final state” (Mar. 2013).
 - [10] The CMS Collaboration, CMS PAS HIG-13-004, “Search for the Standard-Model Higgs boson decaying to tau pairs in proton-proton collisions at $\sqrt{s} = 7$ and 8 TeV” (Mar. 2013).

- [11] Aurelio Juste, “Standard Model Higgs boson searches at the Tevatron”, talk at HCP2012, 15 Nov 2012, Kyoto, Japan,
<http://kds.kek.jp/conferenceDisplay.py?confId=9237>.
- [12] Yuji Enari, “ $H \rightarrow b\bar{b}$ from Tevatron”, talk at HCP2012, 14 Nov 2012, Kyoto, Japan,
<http://kds.kek.jp/conferenceDisplay.py?confId=10808>.
- [13] D. Carmi, A. Falkowski, E. Kuflik and T. Volansky, JHEP **1207**, 136 (2012) [arXiv:1202.3144 [hep-ph]].
- [14] A. Azatov, R. Contino and J. Galloway, JHEP **1204**, 127 (2012) [arXiv:1202.3415 [hep-ph]].
- [15] J. R. Espinosa, C. Grojean, M. Muhlleitner and M. Trott, JHEP **1205**, 097 (2012) [arXiv:1202.3697 [hep-ph]].
- [16] M. Klute, R. Lafaye, T. Plehn, M. Rauch and D. Zerwas, Phys. Rev. Lett. **109**, 101801 (2012) [arXiv:1205.2699 [hep-ph]].
- [17] D. Carmi, A. Falkowski, E. Kuflik and T. Volansky, arXiv:1206.4201 [hep-ph].
- [18] I. Low, J. Lykken and G. Shaughnessy, Phys. Rev. D **86**, 093012 (2012) [arXiv:1207.1093 [hep-ph]].
- [19] P. P. Giardino, K. Kannike, M. Raidal and A. Strumia, Phys. Lett. B **718**, 469 (2012) [arXiv:1207.1347 [hep-ph]].
- [20] J. Ellis and T. You, JHEP **1209**, 123 (2012) [arXiv:1207.1693 [hep-ph]].
- [21] J. R. Espinosa, C. Grojean, M. Muhlleitner and M. Trott, JHEP **1212**, 045 (2012) [arXiv:1207.1717 [hep-ph]].
- [22] D. Carmi, A. Falkowski, E. Kuflik, T. Volansky and J. Zupan, JHEP **1210**, 196 (2012) [arXiv:1207.1718 [hep-ph]].
- [23] S. Banerjee, S. Mukhopadhyay and B. Mukhopadhyaya, JHEP **1210**, 062 (2012) [arXiv:1207.3588 [hep-ph]].
- [24] F. Bonnet, T. Ota, M. Rauch and W. Winter, Phys. Rev. D **86**, 093014 (2012) [arXiv:1207.4599 [hep-ph]].
- [25] T. Plehn and M. Rauch, Europhys. Lett. **100**, 11002 (2012) [arXiv:1207.6108 [hep-ph]].
- [26] A. Djouadi, arXiv:1208.3436 [hep-ph].
- [27] B. A. Dobrescu and J. D. Lykken, arXiv:1210.3342 [hep-ph].
- [28] G. Cacciapaglia, A. Deandrea, G. D. La Rochelle and J. -B. Flament, arXiv:1210.8120 [hep-ph].

- [29] G. Belanger, B. Dumont, U. Ellwanger, J. F. Gunion and S. Kraml, arXiv:1212.5244 [hep-ph].
- [30] G. Moreau, Phys. Rev. D **87**, 015027 (2013) [arXiv:1210.3977 [hep-ph]].
- [31] P. P. Giardino, K. Kannike, I. Masina, M. Raidal and A. Strumia, arXiv:1303.3570 [hep-ph].
- [32] P. Bechtle, S. Heinemeyer, O. Stl, T. Stefaniak and G. Weiglein, arXiv:1305.1933 [hep-ph].
- [33] A. Djouadi and G. g. Moreau, arXiv:1303.6591 [hep-ph].
- [34] A. Falkowski, F. Riva and A. Urbano, arXiv:1303.1812 [hep-ph].
- [35] T. Corbett, O. J. P. Eboli, J. Gonzalez-Fraile and M. C. Gonzalez-Garcia, Phys. Rev. D **86**, 075013 (2012) [arXiv:1207.1344 [hep-ph]].
- [36] T. Corbett, O. J. P. Eboli, J. Gonzalez-Fraile and M. C. Gonzalez-Garcia, Phys. Rev. D **87**, 015022 (2013) [arXiv:1211.4580 [hep-ph]].
- [37] E. Masso and V. Sanz, arXiv:1211.1320 [hep-ph].
- [38] E. Boos, V. Bunichev, M. Dubinin and Y. Kurihara, arXiv:1309.5410 [hep-ph].
- [39] S. Banerjee, S. Mukhopadhyay and B. Mukhopadhyaya, arXiv:1308.4860 [hep-ph].
- [40] J. Cao, P. Wan, J. M. Yang and J. Zhu, JHEP **1308**, 009 (2013) [arXiv:1303.2426 [hep-ph]].
- [41] H. S. Cheon and S. K. Kang, arXiv:1207.1083 [hep-ph].
- [42] N. Craig and S. Thomas, JHEP **1211**, 083 (2012) [arXiv:1207.4835 [hep-ph]].
- [43] D. S. M. Alves, P. J. Fox and N. J. Weiner, arXiv:1207.5499 [hep-ph].
- [44] W. Altmannshofer, S. Gori and G. D. Kribs, Phys. Rev. D **86**, 115009 (2012) [arXiv:1210.2465 [hep-ph]].
- [45] S. Chang, S. K. Kang, J. -P. Lee, K. Y. Lee, S. C. Park and J. Song, arXiv:1210.3439 [hep-ph].
- [46] Y. Bai, V. Barger, L. L. Everett and G. Shaughnessy, arXiv:1210.4922 [hep-ph].
- [47] A. Drozd, B. Grzadkowski, J. F. Gunion and Y. Jiang, arXiv:1211.3580 [hep-ph].
- [48] A. Celis, V. Ilisie and A. Pich, arXiv:1302.4022 [hep-ph].
- [49] C. -W. Chiang and K. Yagyu, JHEP **1307**, 160 (2013) [arXiv:1303.0168 [hep-ph]].
- [50] B. Grinstein and P. Uttayarat, JHEP **1306**, 094 (2013) [Erratum-ibid. **1309**, 110 (2013)] [arXiv:1304.0028 [hep-ph]].
- [51] C. -Y. Chen, S. Dawson and M. Sher, Phys. Rev. D **88**, 015018 (2013) [arXiv:1305.1624 [hep-ph]].
- [52] O. Eberhardt, U. Nierste and M. Wiebusch, arXiv:1305.1649 [hep-ph].
- [53] N. Craig, J. Galloway and S. Thomas, arXiv:1305.2424 [hep-ph].
- [54] G. Belanger, B. Dumont, U. Ellwanger, J. F. Gunion and S. Kraml, arXiv:1306.2941 [hep-ph].

- [55] D. Lopez-Val, T. Plehn and M. Rauch, arXiv:1308.1979 [hep-ph].
- [56] V. Barger, L. L. Everett, H. E. Logan and G. Shaughnessy, arXiv:1308.0052 [hep-ph].
- [57] S. Choi, S. Jung and P. Ko, arXiv:1307.3948 [hep-ph].
- [58] S. Chang, S. K. Kang, J. -P. Lee, K. Y. Lee, S. C. Park and J. Song, arXiv:1310.3374 [hep-ph].
- [59] J. R. Espinosa, C. Grojean, V. Sanz and M. Trott, JHEP **1212**, 077 (2012) [arXiv:1207.7355 [hep-ph]].
- [60] A. Azatov, S. Chang, N. Craig and J. Galloway, Phys. Rev. D **86**, 075033 (2012) [arXiv:1206.1058 [hep-ph]].
- [61] P. Bechtle, S. Heinemeyer, O. Stal, T. Stefaniak, G. Weiglein and L. Zeune, arXiv:1211.1955 [hep-ph].
- [62] J. Cao, Z. Heng, J. M. Yang and J. Zhu, JHEP **1210**, 079 (2012) [arXiv:1207.3698 [hep-ph]].
- [63] H. Baer, V. Barger, P. Huang, D. Mickelson, A. Mustafayev and X. Tata, arXiv:1210.3019 [hep-ph].
- [64] S. L. Glashow and S. Weinberg, “Natural Conservation Laws for Neutral Currents,” Phys. Rev. D **15** (1977) 1958.
- [65] J. S. Lee, A. Pilaftsis, M. S. Carena, S. Y. Choi, M. Drees, J. R. Ellis and C. E. M. Wagner, “CPsuperH: A Computational tool for Higgs phenomenology in the minimal supersymmetric standard model with explicit CP violation,” Comput. Phys. Commun. **156** (2004) 283 [hep-ph/0307377].
- [66] J. S. Lee, M. Carena, J. Ellis, A. Pilaftsis and C. E. M. Wagner, “CPsuperH2.0: an Improved Computational Tool for Higgs Phenomenology in the MSSM with Explicit CP Violation,” Comput. Phys. Commun. **180** (2009) 312 [arXiv:0712.2360 [hep-ph]].
- [67] J. S. Lee, M. Carena, J. Ellis, A. Pilaftsis and C. E. M. Wagner, “CPsuperH2.3: an Updated Tool for Phenomenology in the MSSM with Explicit CP Violation,” Comput. Phys. Commun. **184**, 1220 (2013) [arXiv:1208.2212 [hep-ph]].
- [68] R. A. Battye, G. D. Brawn, A. Pilaftsis, “Vacuum Topology of the Two Higgs Doublet Model,” JHEP **1108** (2011) 020. [arXiv:1106.3482 [hep-ph]].
- [69] S. Davidson and H. E. Haber, “Basis-independent methods for the two-Higgs-doublet model,” Phys. Rev. D **72** (2005) 035004 [Erratum-ibid. D **72** (2005) 099902] [hep-ph/0504050].
- [70] S.Y. Choi and J.S. Lee, Phys. Rev. **D61** (2000) 015003; S.Y. Choi, K. Hagiwara and J.S. Lee, Phys. Rev. **D64** (2001) 032004; S. Y. Choi, M. Drees, J. S. Lee and J. Song, Eur. Phys. J. C

25 (2002) 307.

[71] ATLAS Collaboration, ATLAS-CONF-2013-013; ATLAS-CONF-2013-067.

[72] CMS Collaboration, Eur. Phys. J. C 73 (2013) 2469 [arXiv:1304.0213 [hep-ex]]; CMS-HIG-12-024 (July 24, 2013).

[73] ATLAS Collaboration, JHEP **1302** (2013) 095, [arXiv:1211.6956 [hep-ex]].

[74] A. Celis, V. Ilisie, A. Pich, “Towards a general analysis of LHC data within two-Higgs-doublet models,” [arXiv:1310.7941 [hep-ph]].

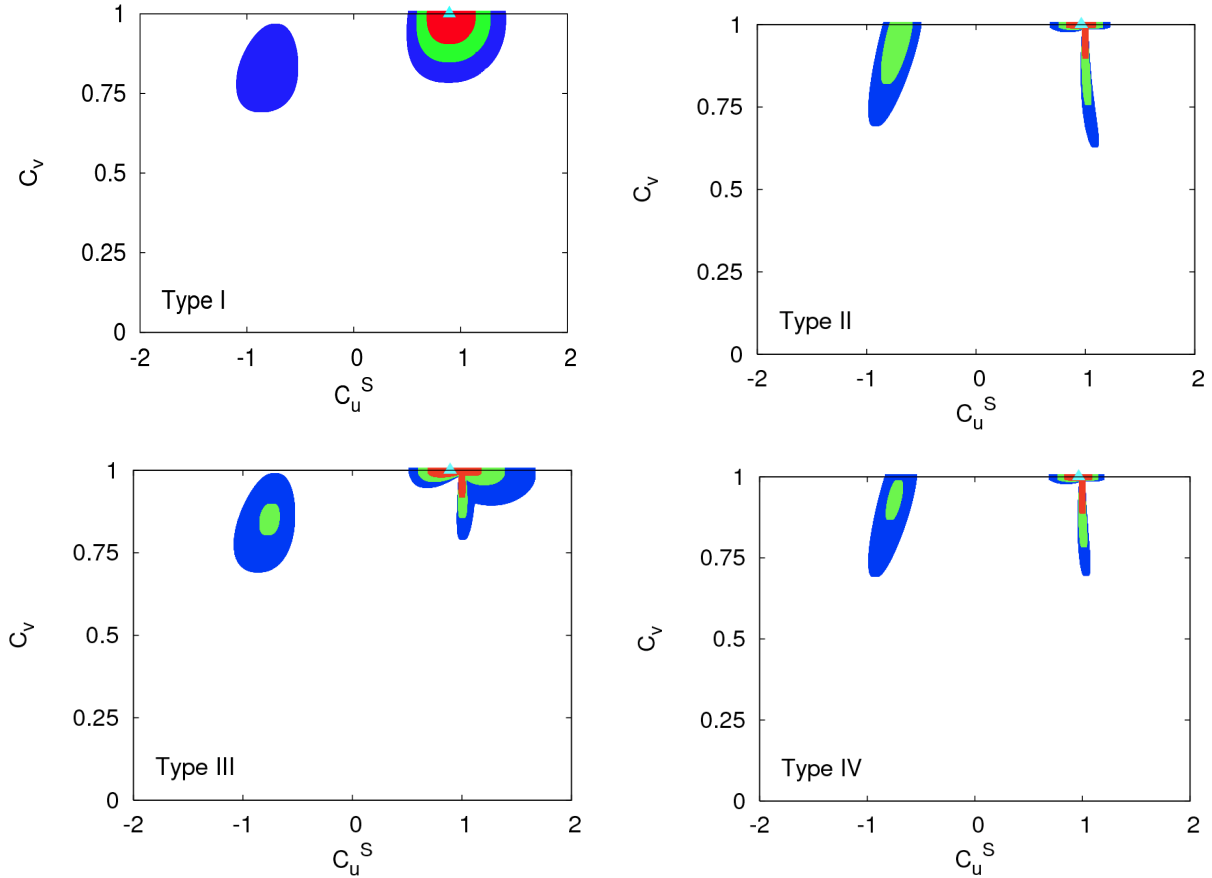


FIG. 2. The confidence-level regions of the fit by varying C_u^S and C_v (or equivalently $\log_{10} \tan \beta$) only (**CPC2** case) in the plane of C_u^S vs C_v for Type I – IV. The contour regions shown are for $\Delta\chi^2 \leq 2.3$ (red), 5.99 (green), and 11.83 (blue) above the minimum, which correspond to confidence levels of 68.3%, 95%, and 99.7%, respectively. The best-fit points are denoted by the triangle.

TABLE III. The best-fit values for various CPC and CPV fits. The SM values are: $\chi^2 = 18.94$, $\chi^2/\text{dof} = 0.86$, and $p\text{-value} = 0.65$.

Fits	Type	χ^2	χ^2/dof	$p\text{-value}$	Best-fit values				
					C_u^S	C_u^P	C_v	$\tan\beta$	$(\Delta S^\gamma)^{H^\pm}$
CPC2	I	18.39	0.920	0.562	0.895	0	1.000	<i>limit</i>	0
	II	18.68	0.934	0.543	0.963	0	1.000	<i>limit</i>	0
	III	18.44	0.922	0.558	0.892	0	1.000	<i>limit</i>	0
	IV	18.66	0.933	0.544	0.965	0	1.000	<i>limit</i>	0
CPC3	I	17.64	0.928	0.547	0.924	0	0.965	6.308	-0.756
	I	17.64	0.928	0.547	-0.921	0	0.965	0.144	2.377
	II	17.30	0.910	0.570	-0.822	0	1.000	2×10^{-4}	2.218
	III	17.63	0.928	0.547	-0.912	0	0.967	0.137	2.365
	IV	17.54	0.923	0.553	0.955	0	1.000	0.662	-0.835
CPV3	I	18.37	0.967	0.498	0.867	0.142	0.988	0.840	0
	I	18.37	0.967	0.498	0.867	-0.142	0.988	0.840	0
	II	17.17	0.904	0.578	0.476	-0.505	0.998	0.082	0
	II	17.17	0.904	0.578	0.475	0.505	0.998	0.095	0
	III	18.41	0.969	0.495	0.873	-0.110	1.000	2×10^{-4}	0
	III	18.41	0.969	0.495	0.873	0.109	1.000	1.2×10^{-4}	0
	IV	18.16	0.956	0.512	0.806	0.339	1.000	<i>limit</i>	0
	IV	18.16	0.956	0.512	0.806	-0.339	1.000	1.2×10^{-4}	0
CPV4	I	17.64	0.980	0.480	0.924	-1.5×10^{-3}	0.964	6.488	-0.777
	I	17.64	0.980	0.480	-0.924	2×10^{-4}	0.965	0.139	2.389
	II	17.07	0.948	0.518	-0.052	0.572	0.999	0.045	1.042
	II	17.07	0.948	0.518	-0.052	-0.572	0.999	0.045	1.042
	III	17.64	0.980	0.480	-0.909	0.032	0.972	0.126	2.370
	IV	17.54	0.975	0.486	0.956	-0.016	1.000	0.670	-0.831

TABLE IV. Table showing the corresponding best-fit values for $C_{d,l}^{S,P}$.

Fits	Type	χ^2	χ^2/dof	p -value	Best-fit values			
					C_d^S	C_l^S	C_d^P	C_l^P
CPC2	I	18.39	0.920	0.562	0.896	0.896	0	0
	II	18.68	0.934	0.543	1.000	1.000	0	0
	III	18.44	0.922	0.558	0.892	1.000	0	0
	IV	18.66	0.933	0.544	1.000	0.965	0	0
CPC3	I	17.64	0.928	0.547	0.923	0.923	0	0
	I	17.64	0.928	0.547	-0.923	-0.923	0	0
	II	17.30	0.910	0.570	1.000	1.000	0	0
	III	17.63	0.928	0.547	-0.914	1.002	0	0
	IV	17.54	0.923	0.553	1.015	0.951	0	0
CPV3	I	18.37	0.967	0.498	0.867	0.867	-0.142	-0.142
	I	18.37	0.967	0.498	0.867	0.867	0.142	0.142
	II	17.17	0.904	0.578	1.002	1.002	-4.6×10^{-3}	-4.6×10^{-3}
	II	17.17	0.904	0.578	1.002	1.002	4.6×10^{-3}	4.6×10^{-3}
	III	18.41	0.969	0.495	0.873	1.000	0.109	0
	III	18.41	0.969	0.495	0.873	1.000	-0.109	0
	IV	18.16	0.956	0.512	1.000	0.806	0	-0.339
	IV	18.16	0.956	0.512	1.000	0.806	0	0.339
CPV4	I	17.64	0.980	0.480	0.924	0.924	1.5×10^{-3}	1.5×10^{-3}
	I	17.64	0.980	0.480	-0.924	-0.924	-2×10^{-4}	-2×10^{-4}
	II	17.07	0.948	0.518	1.001	1.001	1.2×10^{-3}	1.2×10^{-3}
	II	17.07	0.948	0.518	1.001	1.001	-1.2×10^{-3}	-1.2×10^{-3}
	III	17.64	0.980	0.480	-0.914	1.002	-3×10^{-5}	0
	IV	17.54	0.975	0.486	1.015	0.951	-1×10^{-3}	3×10^{-3}

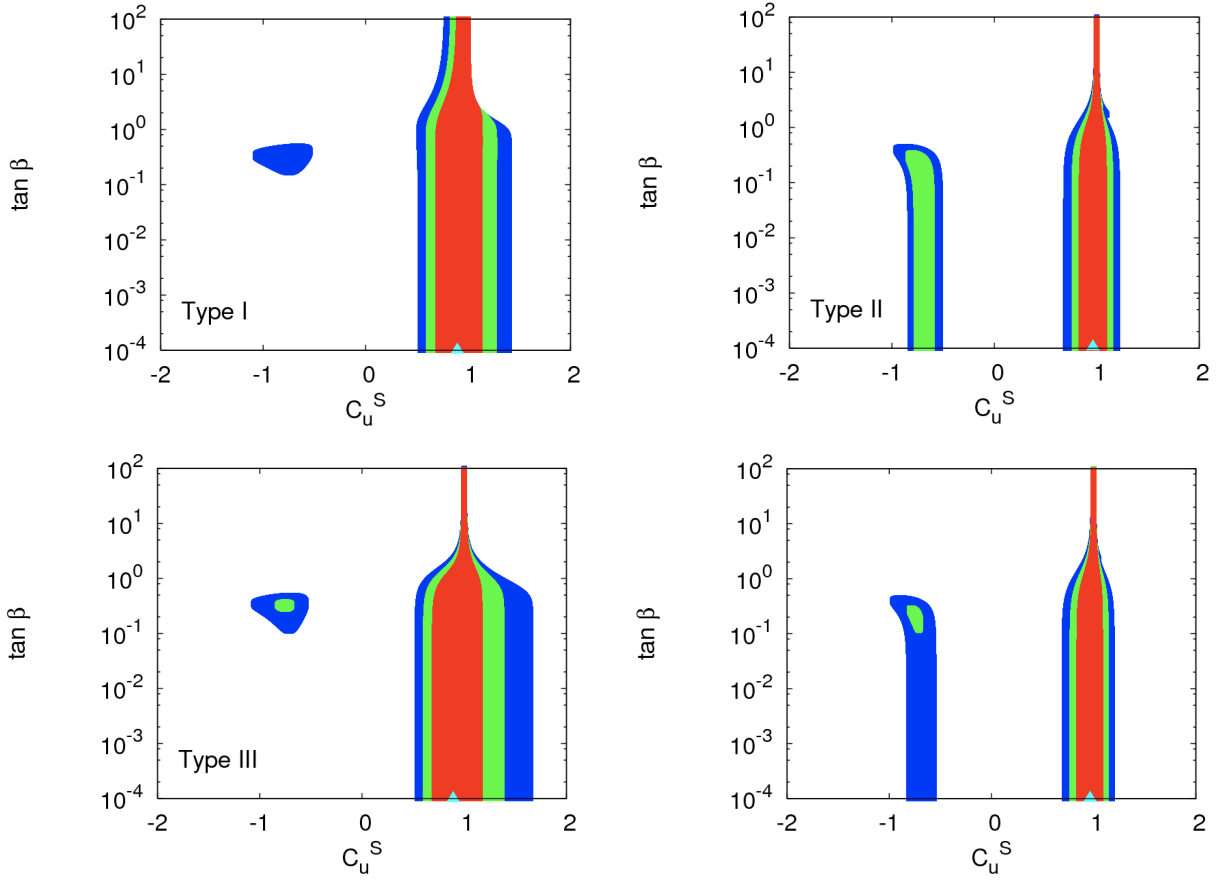


FIG. 3. The same as Fig. 2 but in the plane of C_u^S vs $\tan \beta$ (**CPC2**). The description of the confidence regions is the same as Fig. 2.

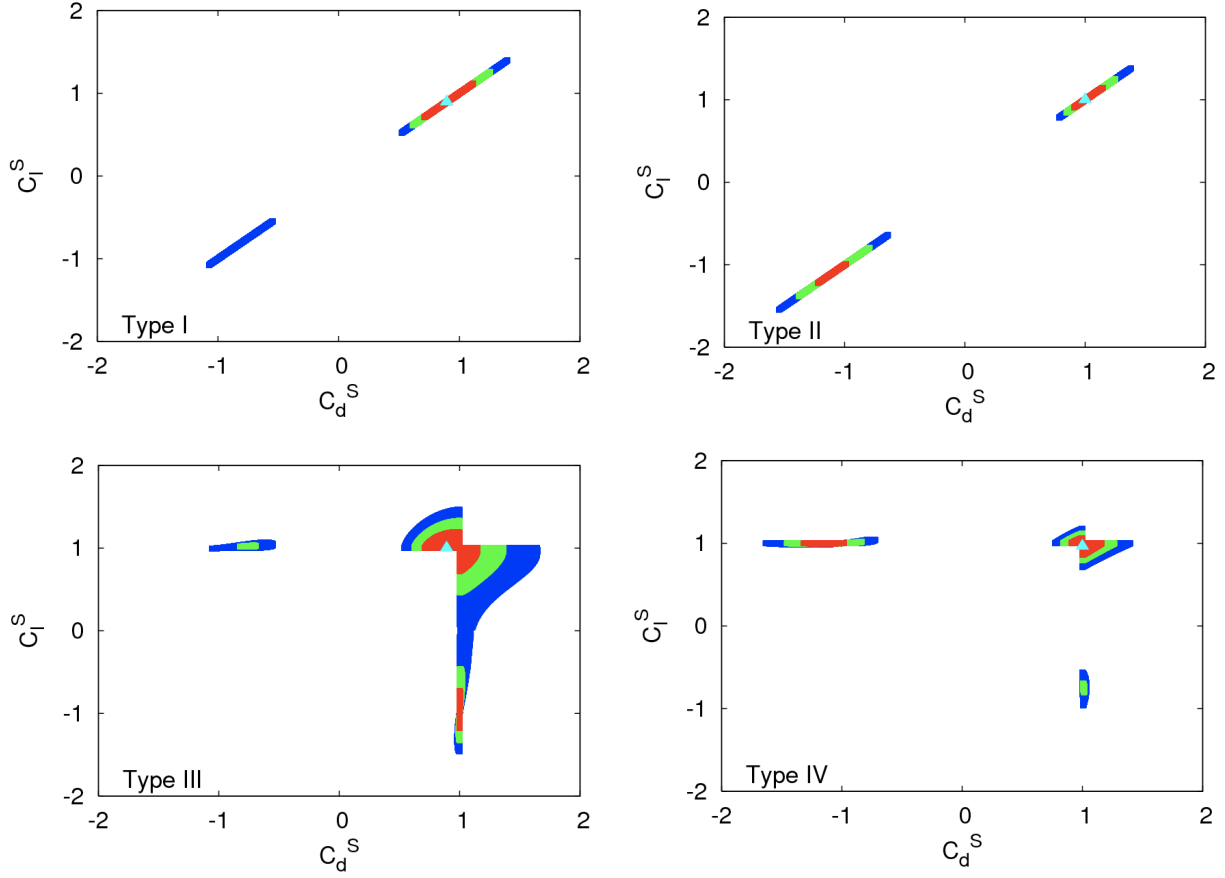


FIG. 4. The same as Fig. 2 but in the plane of C_d^S vs C_l^S (**CPC2**). The description of the confidence regions is the same as Fig. 2.

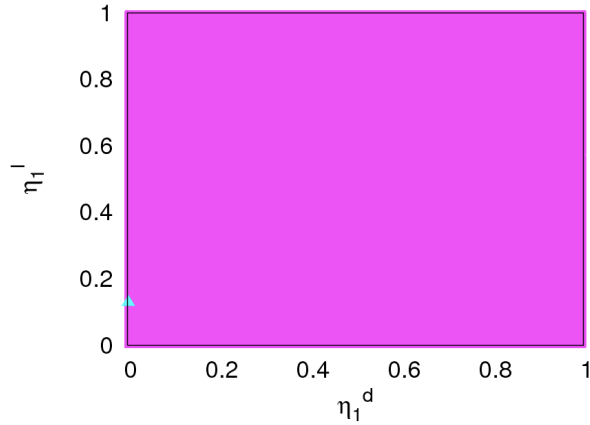


FIG. 5. The confidence-level regions of the fit by varying C_u^S , C_v , η_1^d , and η_1^l in the plane of η_1^d vs η_1^l . The best-fit points are denoted by the triangle. Here the entire region is for $\Delta\chi^2 < 1.0$.

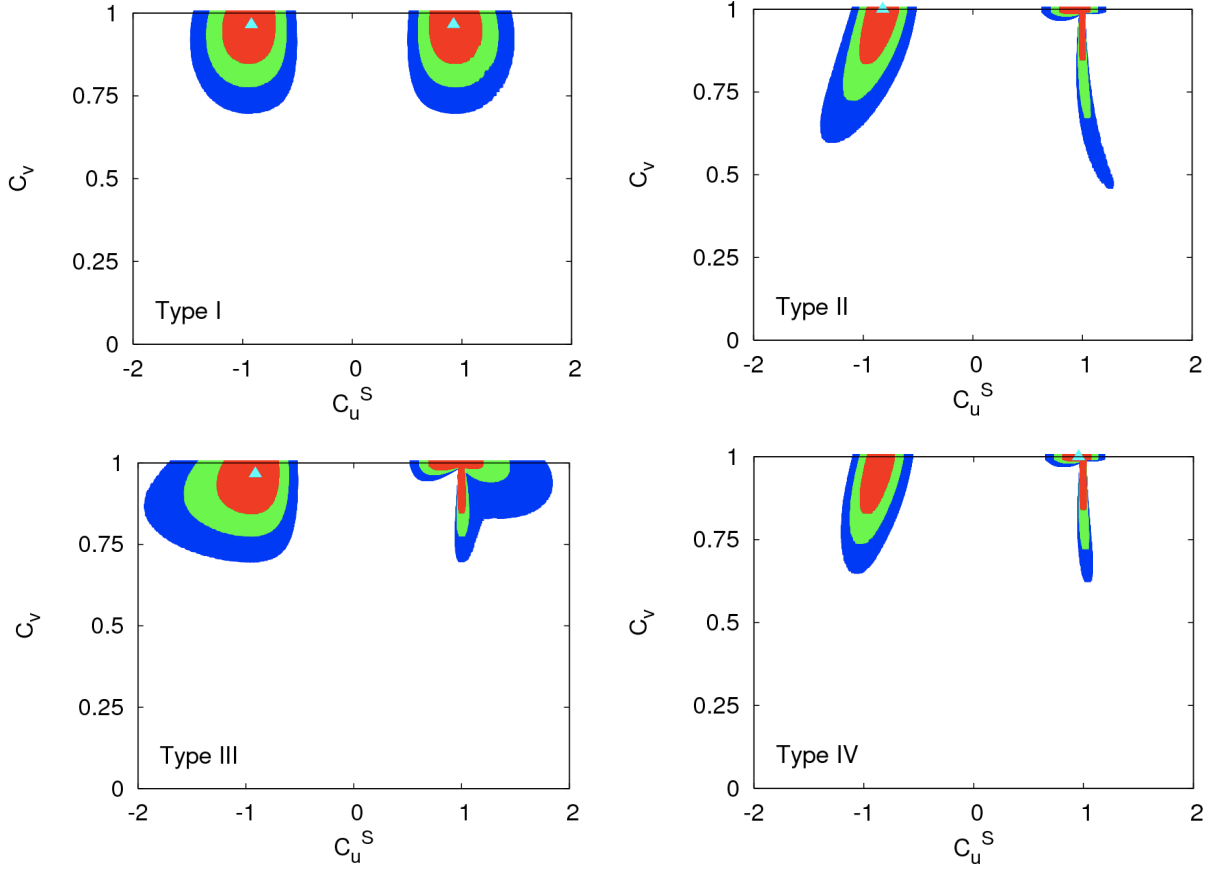


FIG. 6. The confidence-level regions of the fit by varying C_u^S , $\log_{10} \tan \beta$, and ΔS^γ (**CPC3** case) in the plane of C_u^S vs C_v for Type I – IV. The contour regions shown are for $\Delta\chi^2 \leq 2.3$ (red), 5.99 (green), and 11.83 (blue) above the minimum, which correspond to confidence levels of 68.3%, 95%, and 99.7%, respectively. The best-fit points are denoted by the triangle.

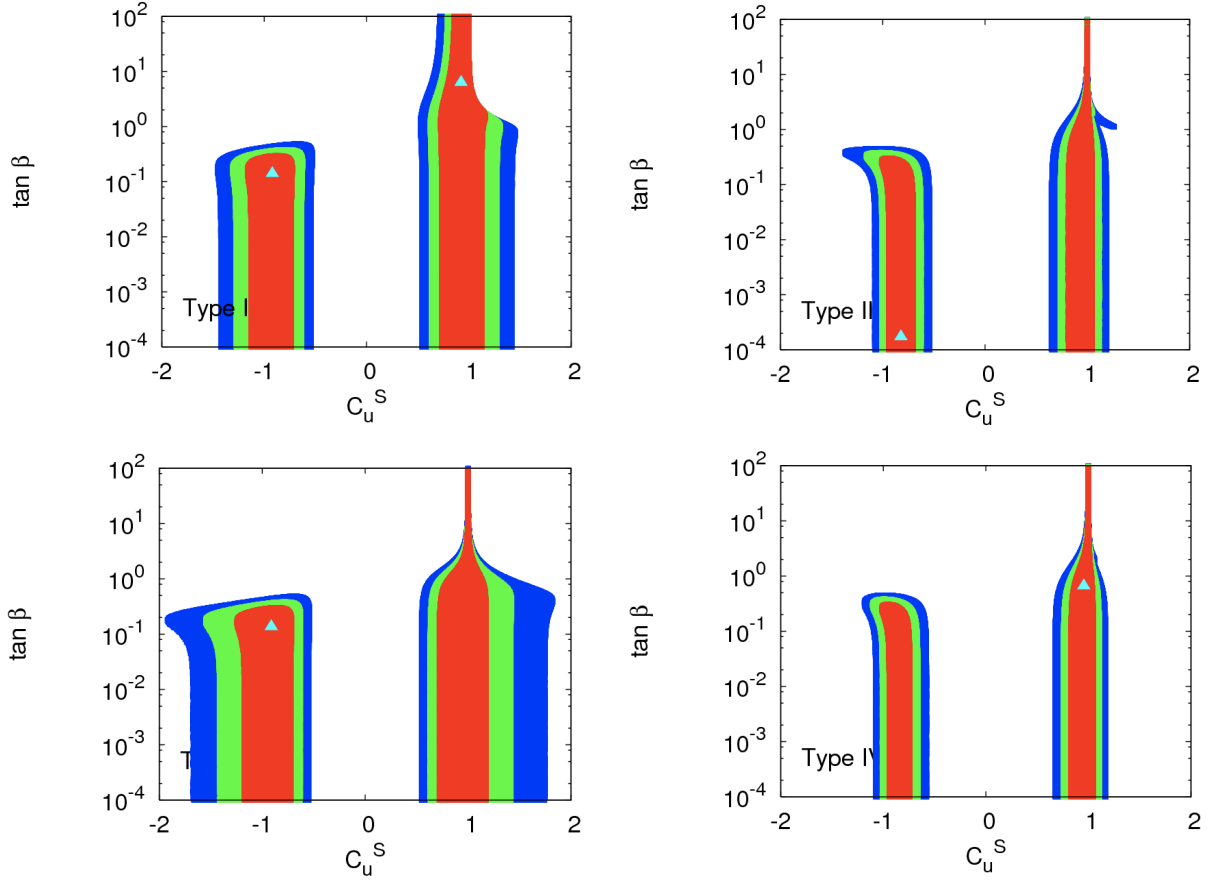


FIG. 7. The same as Fig. 6 but in the plane of C_u^S vs $\tan \beta$ for Type I – IV (**CPC3**). The description of the confidence regions is the same as Fig. 6.

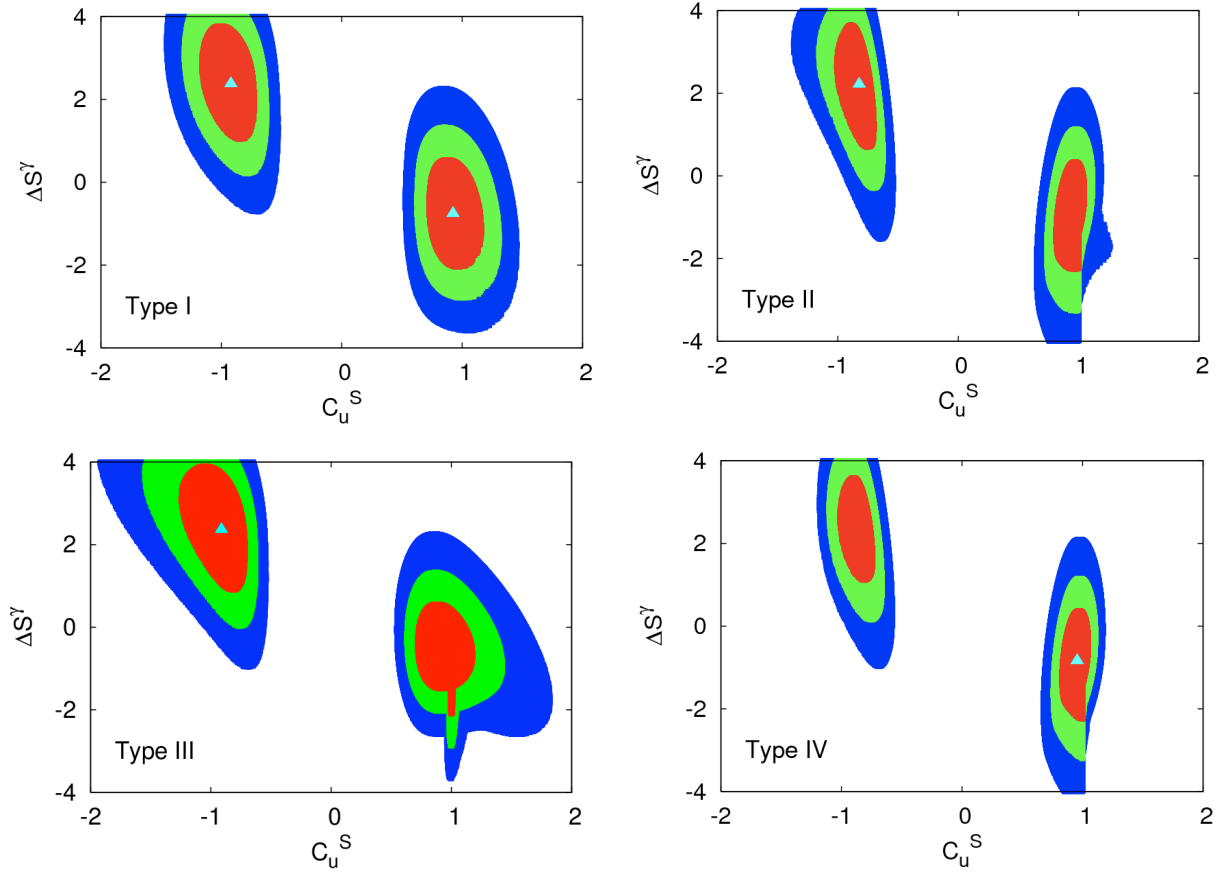


FIG. 8. The same as Fig. 6 but in the plane of C_u^S vs $(\Delta S^\gamma)^{H^\pm}$ for Type I – IV (**CPC3**). The description of the confidence regions is the same as Fig. 6.

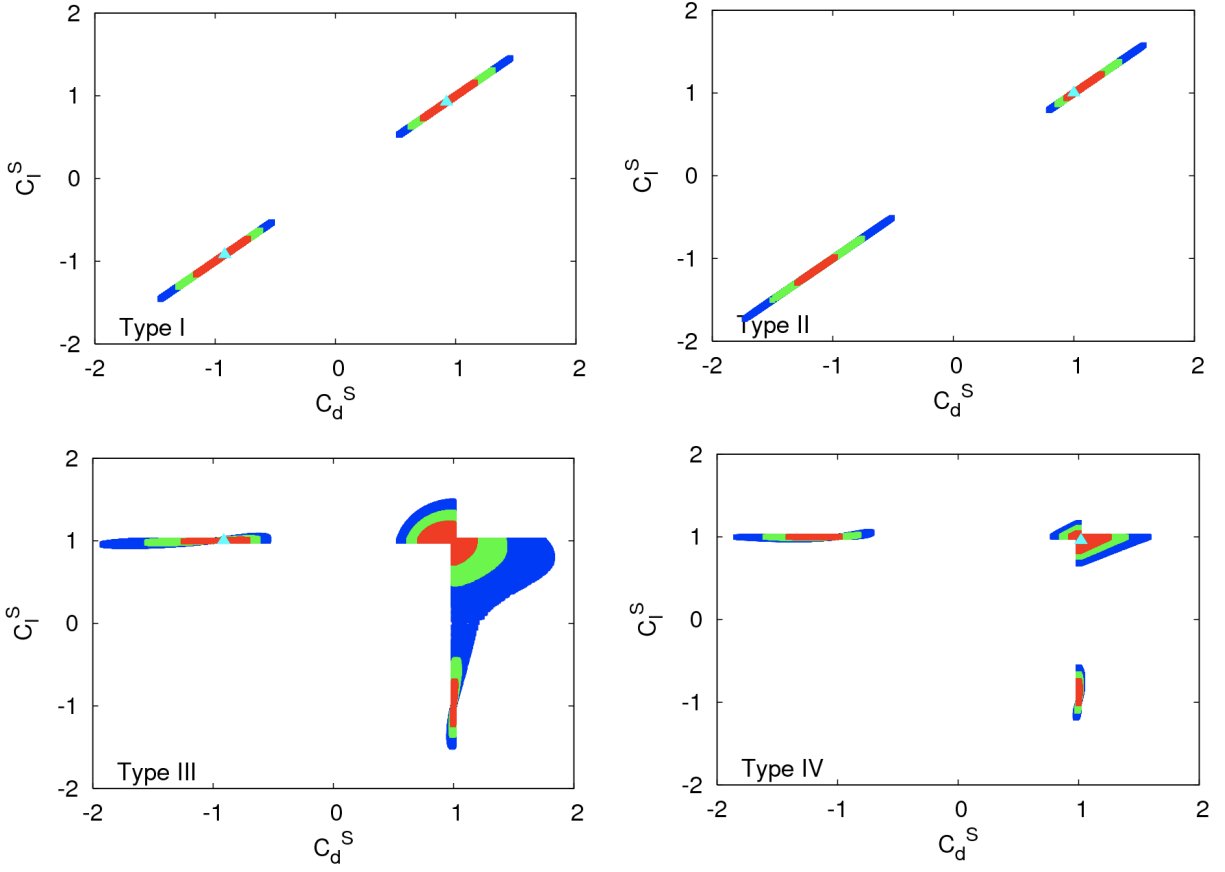


FIG. 9. The same as Fig. 6 but in the plane of C_d^S vs C_l^S for Type I – IV (**CPC3**). The description of the confidence regions is the same as Fig. 6.

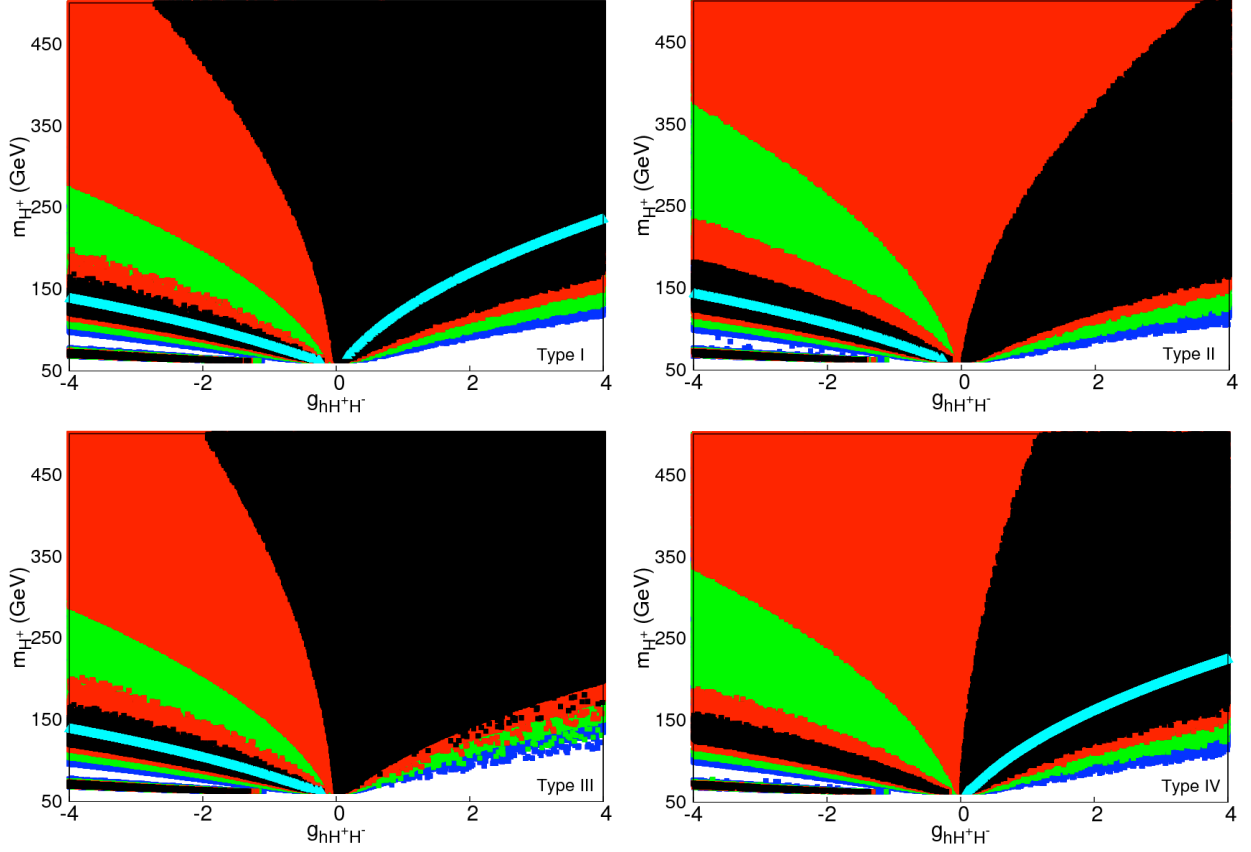


FIG. 10. The same as Fig. 6 but we used $g_{hH^+H^-}$ and m_{H^\pm} in place of $(\Delta S^\gamma)^{H^\pm}$ (CPC3 case) for Type I – IV. The contour regions shown are for $\Delta\chi^2 \leq 1.0$ (black), 2.3 (red), 5.99 (green), and 11.83 (blue) above the minimum, which correspond to confidence levels of 39.3%, 68.3%, 95%, and 99.7%, respectively. The best-fit points are denoted by a beam of cyan triangles.

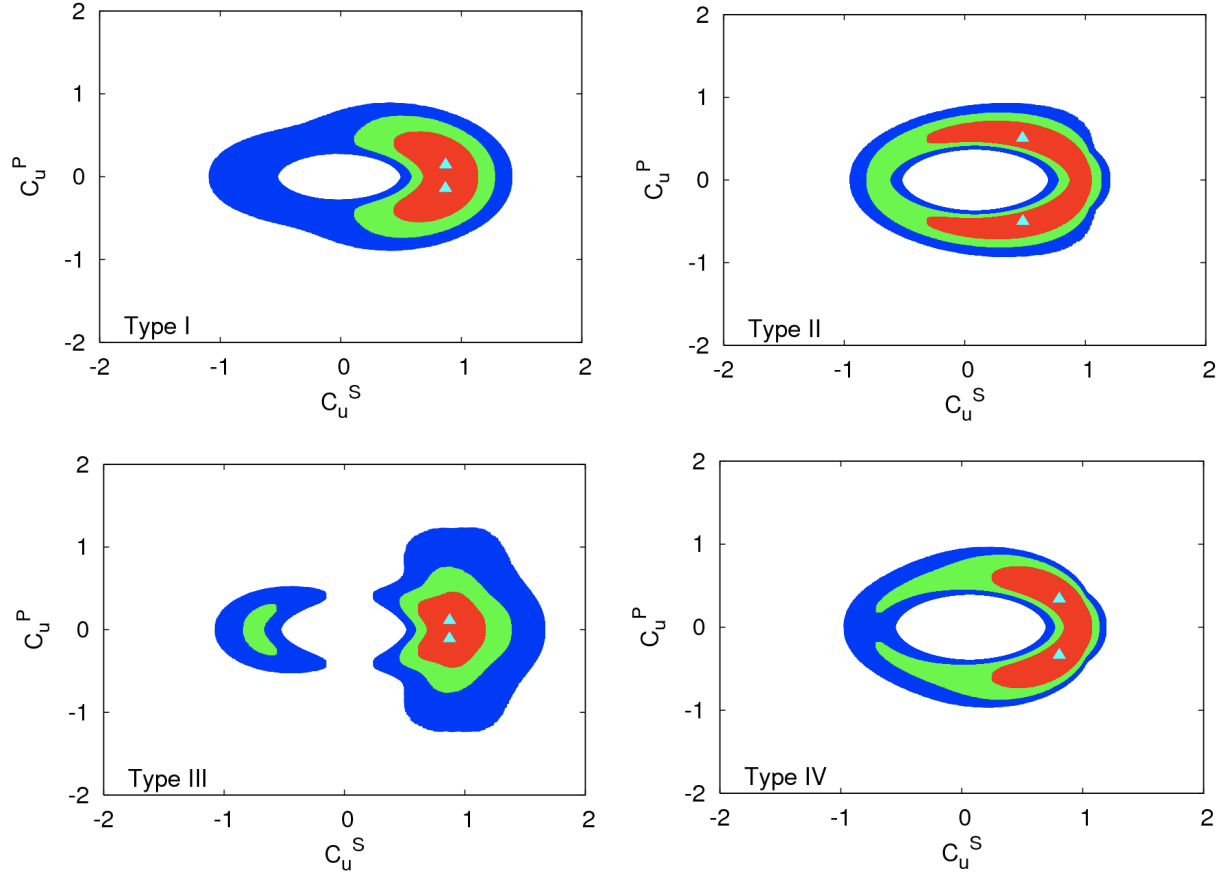


FIG. 11. The confidence-level regions of the fit by varying C_u^S , C_u^P , and $\log_{10} \tan \beta$ (**CPV3** case) in the plane of C_u^S vs C_u^P for Type I – IV. The contour regions shown are for $\Delta\chi^2 \leq 2.3$ (red), 5.99 (green), and 11.83 (blue) above the minimum, which correspond to confidence levels of 68.3%, 95%, and 99.7%, respectively. The best-fit points are denoted by the triangle.

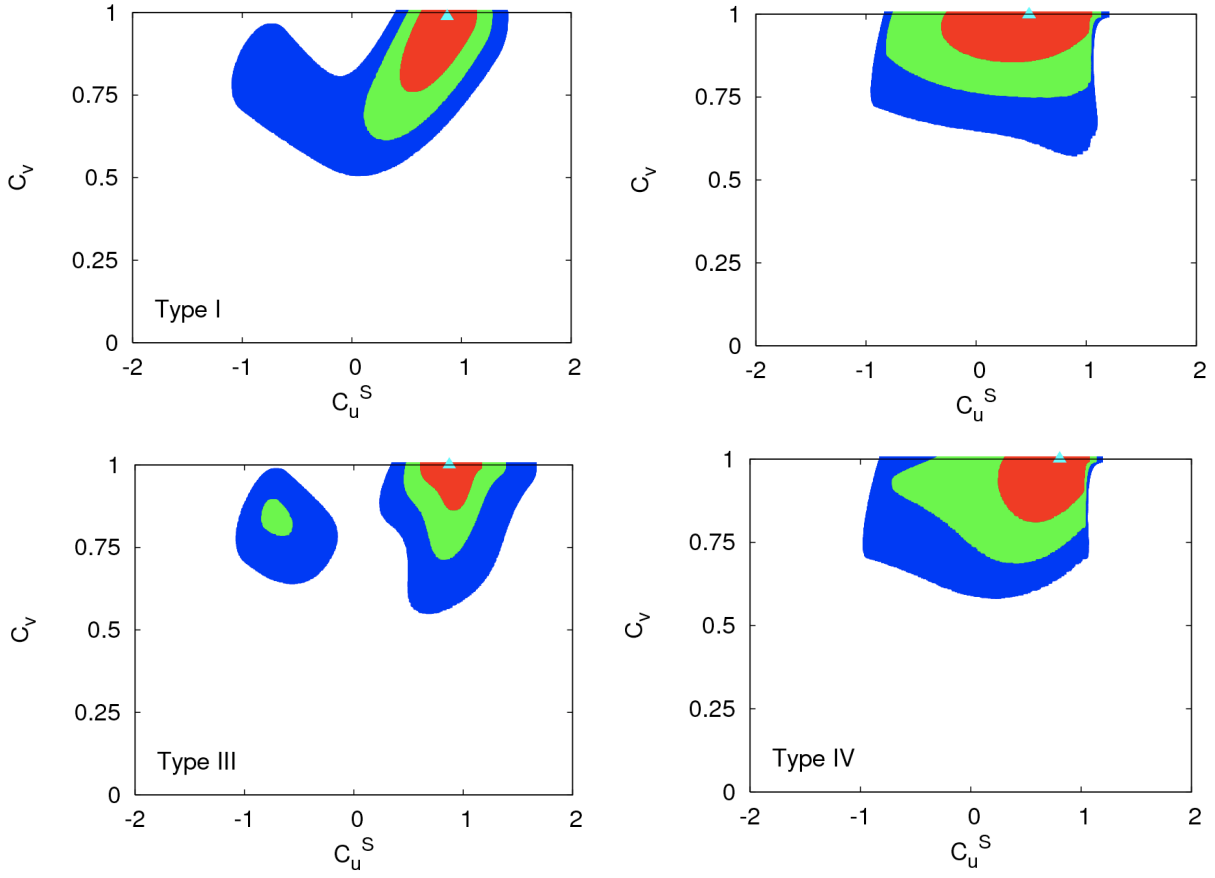


FIG. 12. The same as in Fig. 11 but in the plane of C_u^S vs C_v for Type I – IV (**CPV3**). The description of the confidence regions is the same as Fig. 11.

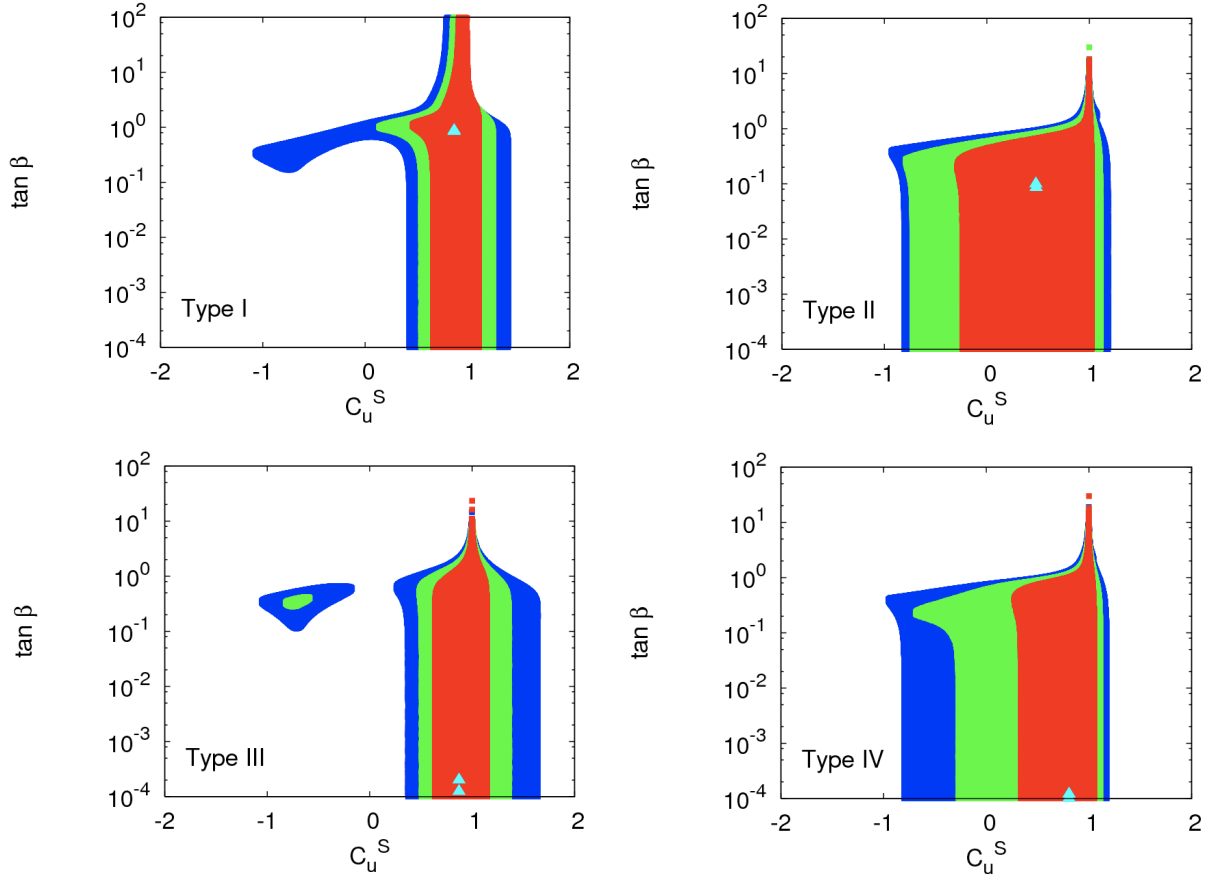


FIG. 13. The same as in Fig. 11 but in the plane of C_u^S vs $\tan \beta$ for Type I – IV (CPV3). The description of the confidence regions is the same as Fig. 11.

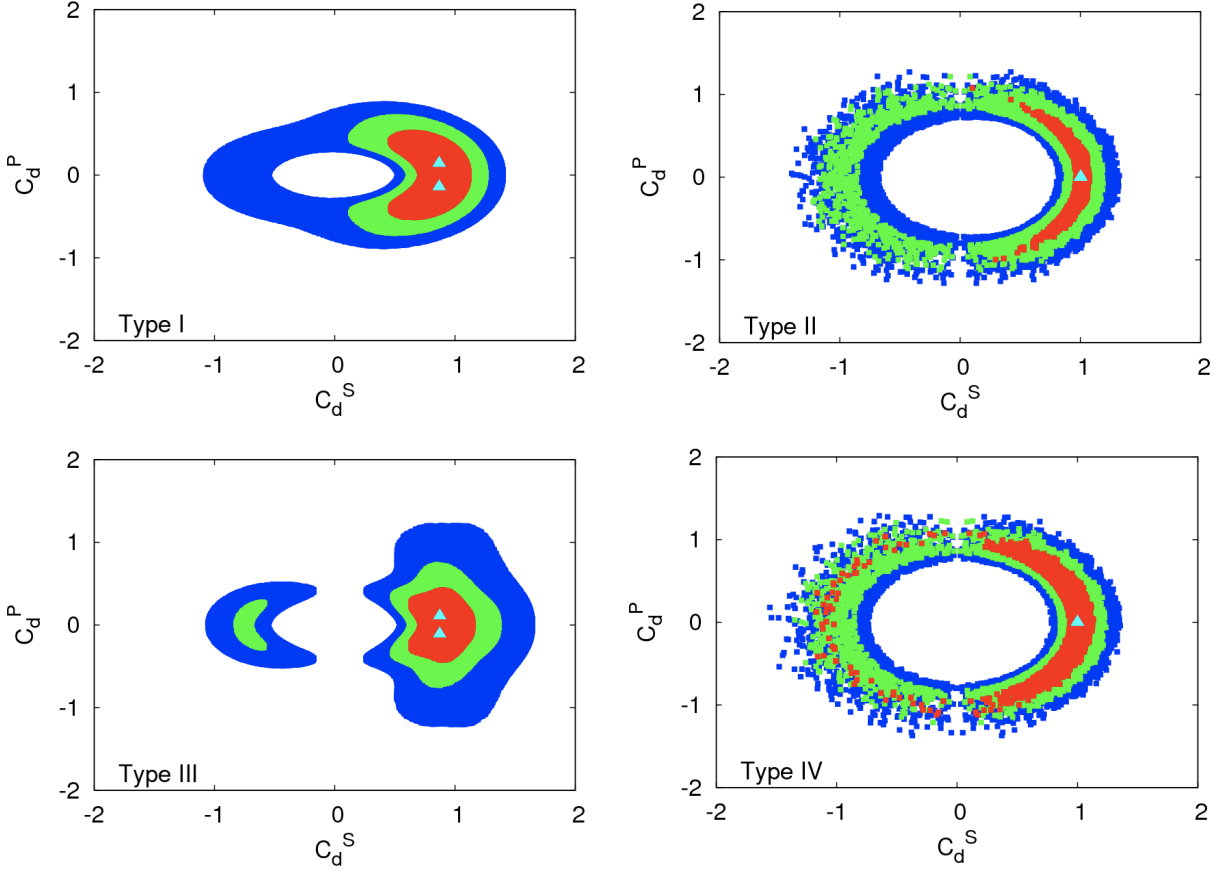


FIG. 14. The same as in Fig. 11 but in the plane of C_d^S vs C_d^P for Type I – IV (**CPV3**). The description of the confidence regions is the same as Fig. 11.

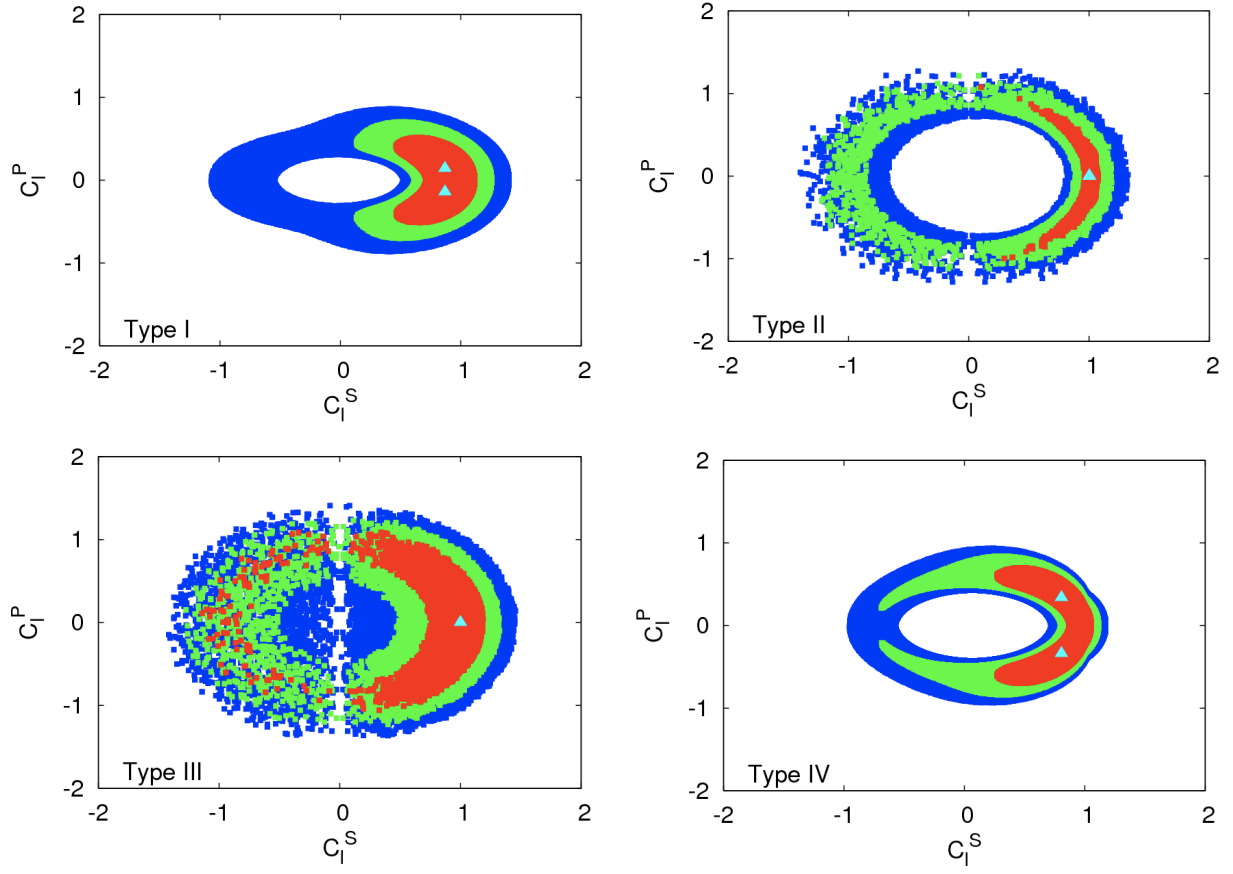


FIG. 15. The same as in Fig. 11 but in the plane of C_1^S vs C_1^P for Type I – IV (**CPV3**). The description of the confidence regions is the same as Fig. 11.

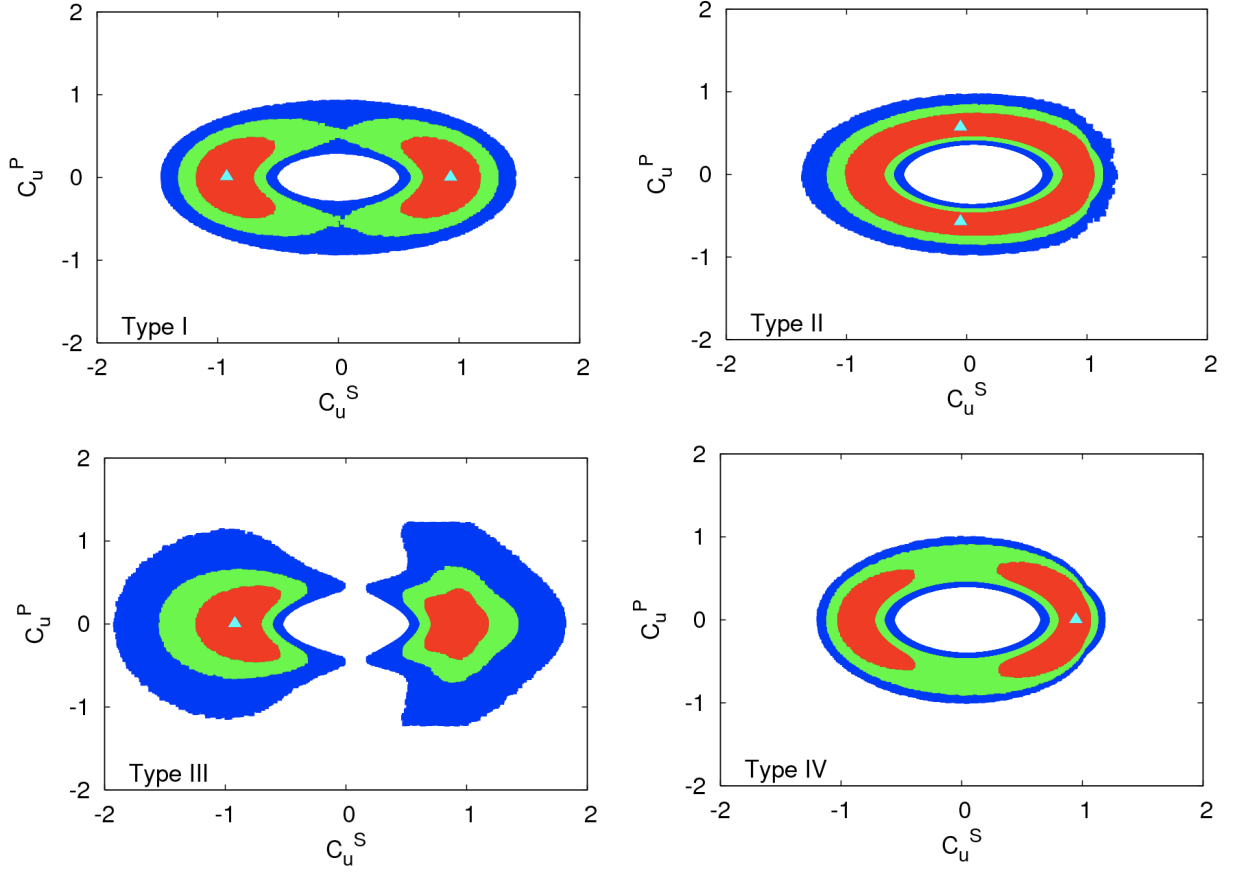


FIG. 16. The confidence-level regions of the fit by varying C_u^S , C_u^P , $\log_{10} \tan \beta$, and $(\Delta S^\gamma)^{H^\pm}$ (CPV4 case) in the plane of C_u^S vs C_u^P for Type I – IV. The contour regions shown are for $\Delta\chi^2 \leq 2.3$ (red), 5.99 (green), and 11.83 (blue) above the minimum, which correspond to confidence levels of 68.3%, 95%, and 99.7%, respectively. The best-fit points are denoted by the triangle.

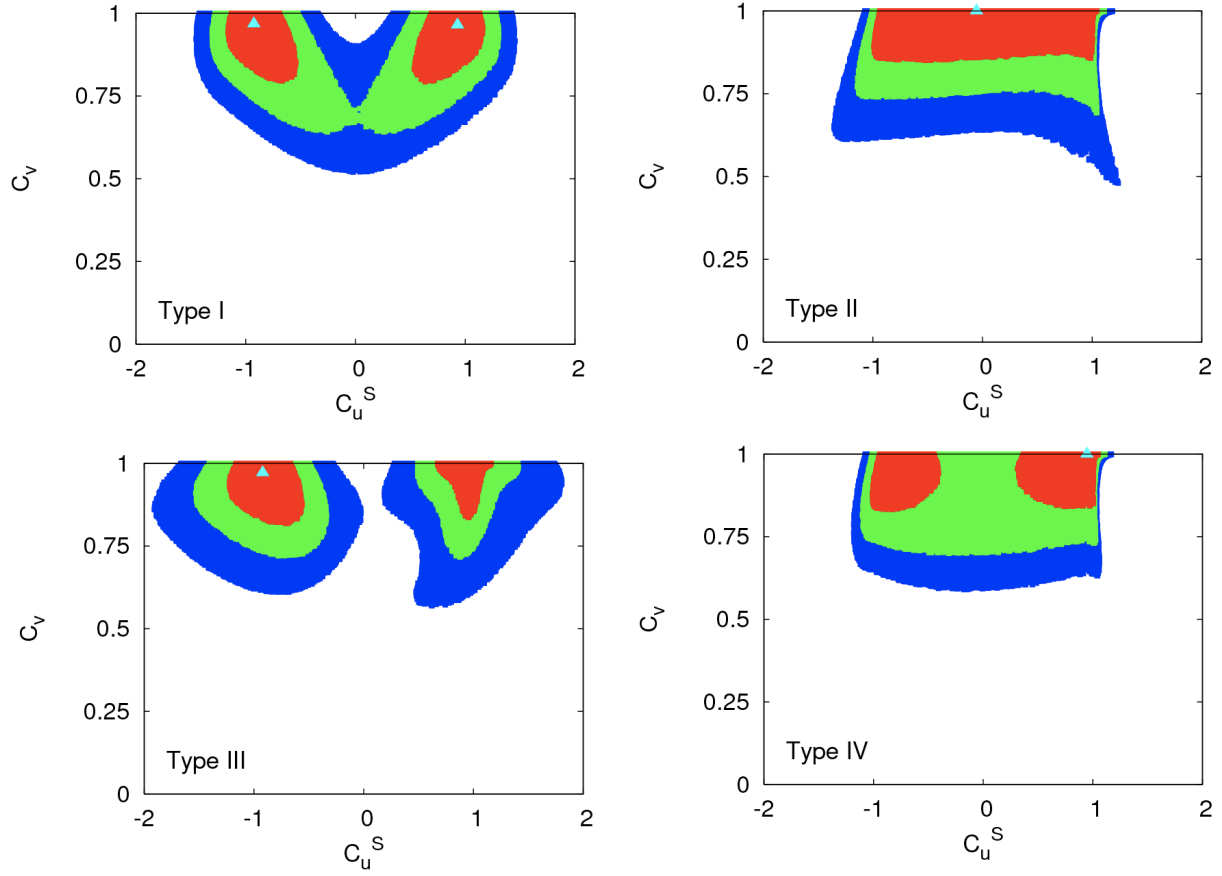


FIG. 17. The same as Fig. 16 but in the plane of C_u^S vs C_v for Type I – IV (**CPV4**). The description of the confidence regions is the same as Fig. 16.

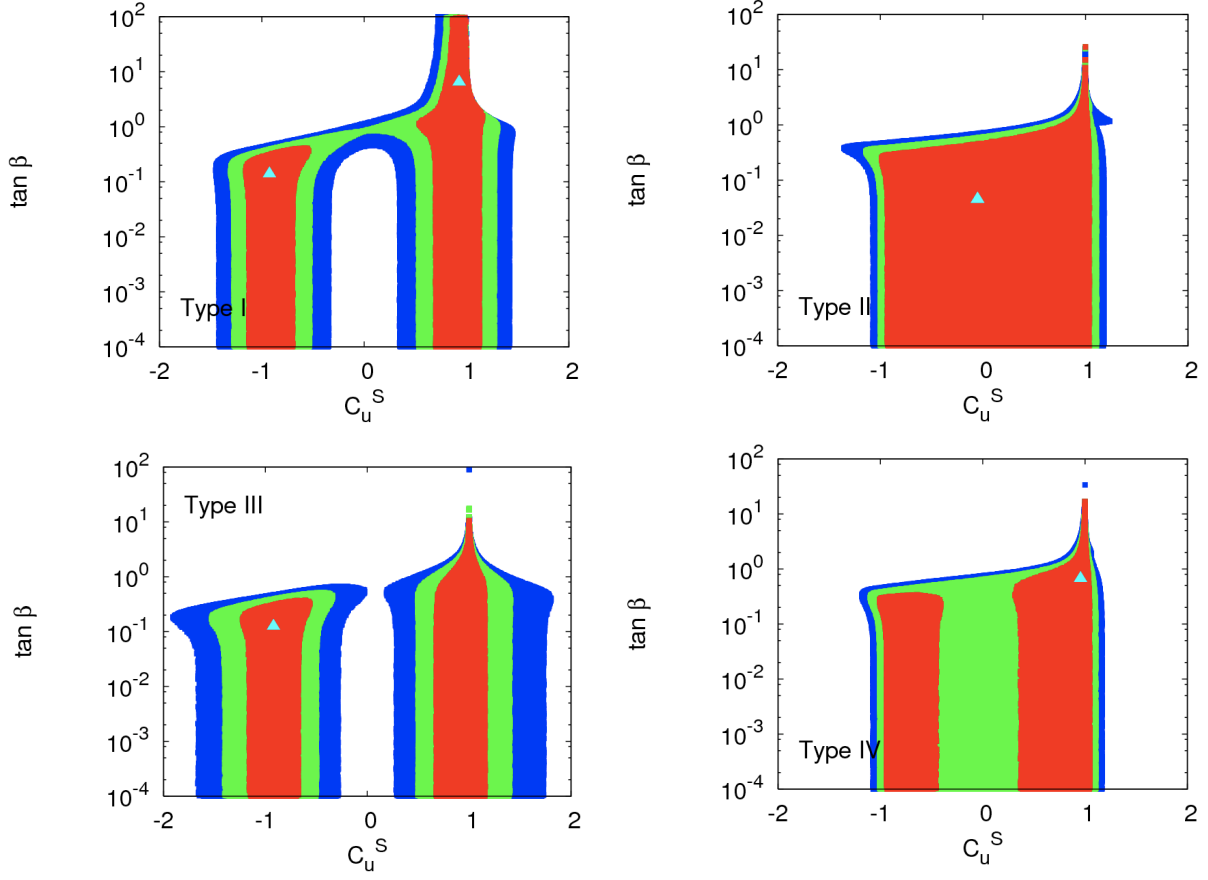


FIG. 18. The same as Fig. 16 but in the plane of C_u^S vs $\tan \beta$ for Type I – IV (CPV4 case). The description of the confidence regions is the same as Fig. 16.

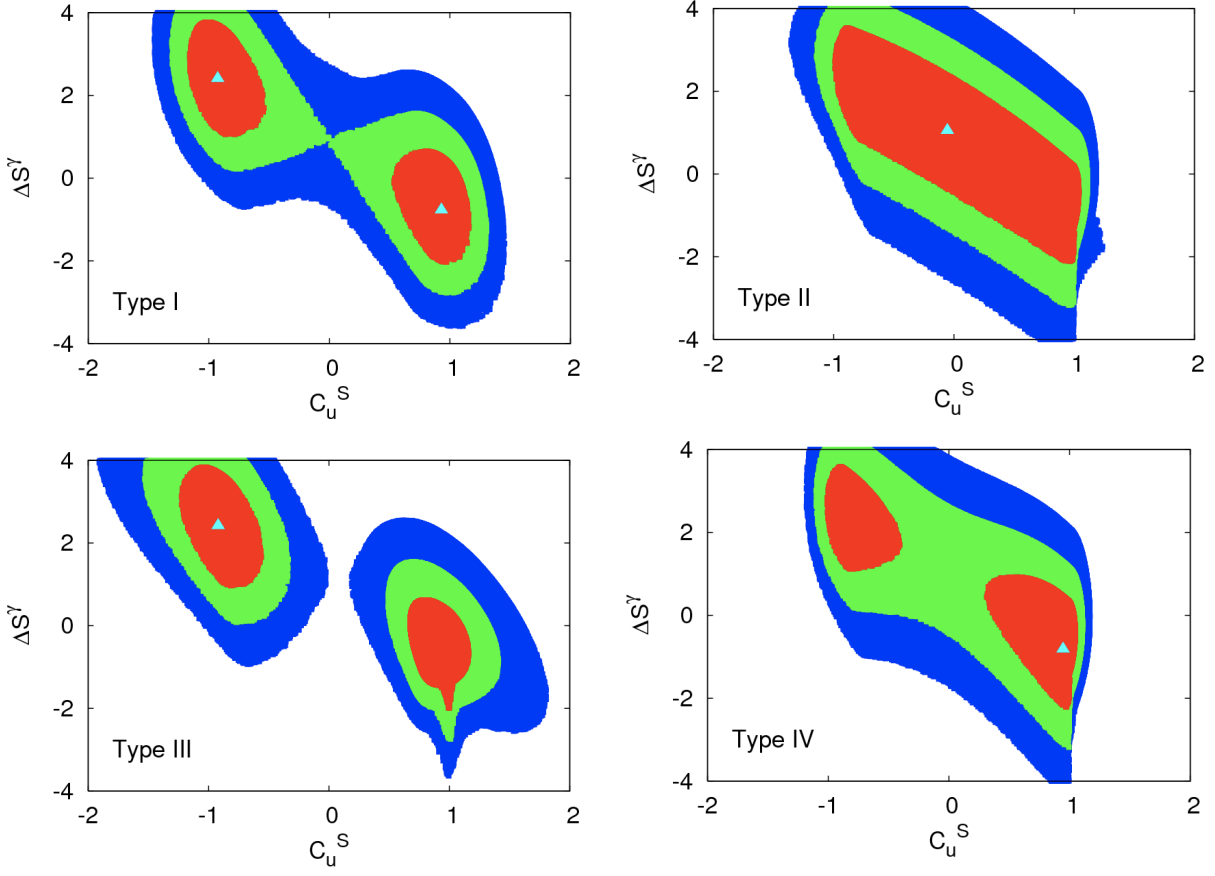


FIG. 19. The same as Fig. 16 but in the plane of C_u^S vs $(\Delta S^\gamma)^{H^\pm}$ for Type I – IV (CPV4). The description of the confidence regions is the same as Fig. 16.

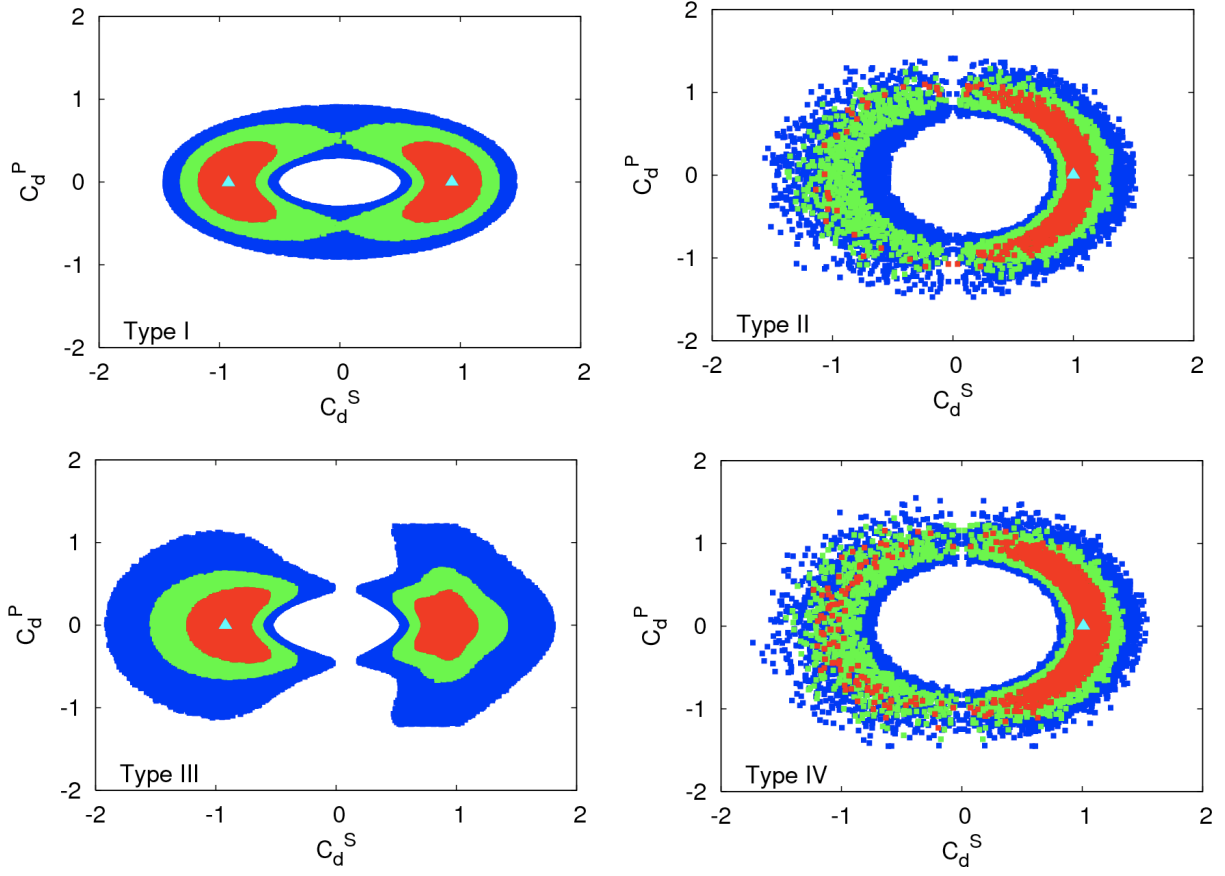


FIG. 20. The same as Fig. 16 but in the plane of C_d^S vs C_d^P for Type I – IV (**CPV4**). The description of the confidence regions is the same as Fig. 16.

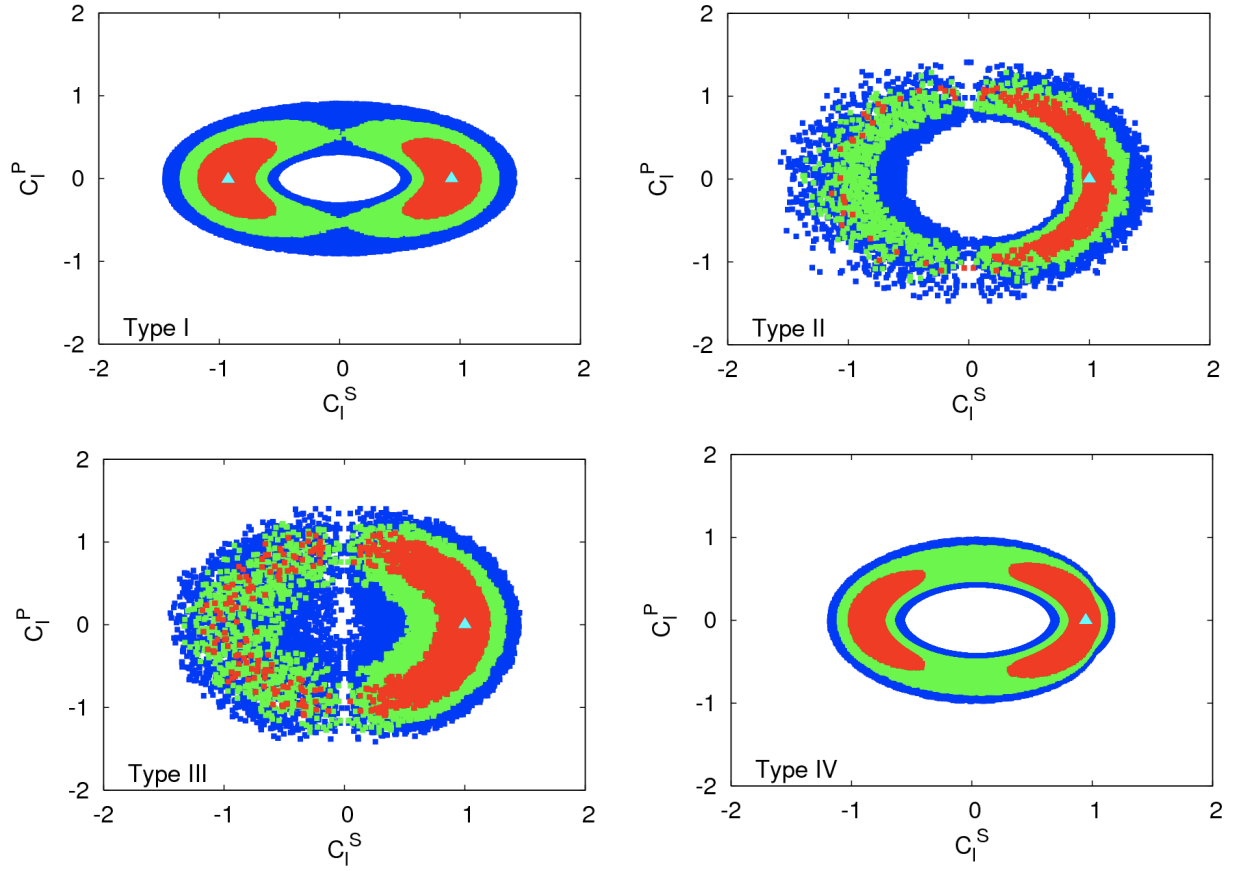


FIG. 21. The same as Fig. 16 but in the plane of C_ℓ^S vs C_ℓ^P for Type I – IV (**CPV4**). The description of the confidence regions is the same as Fig. 16.

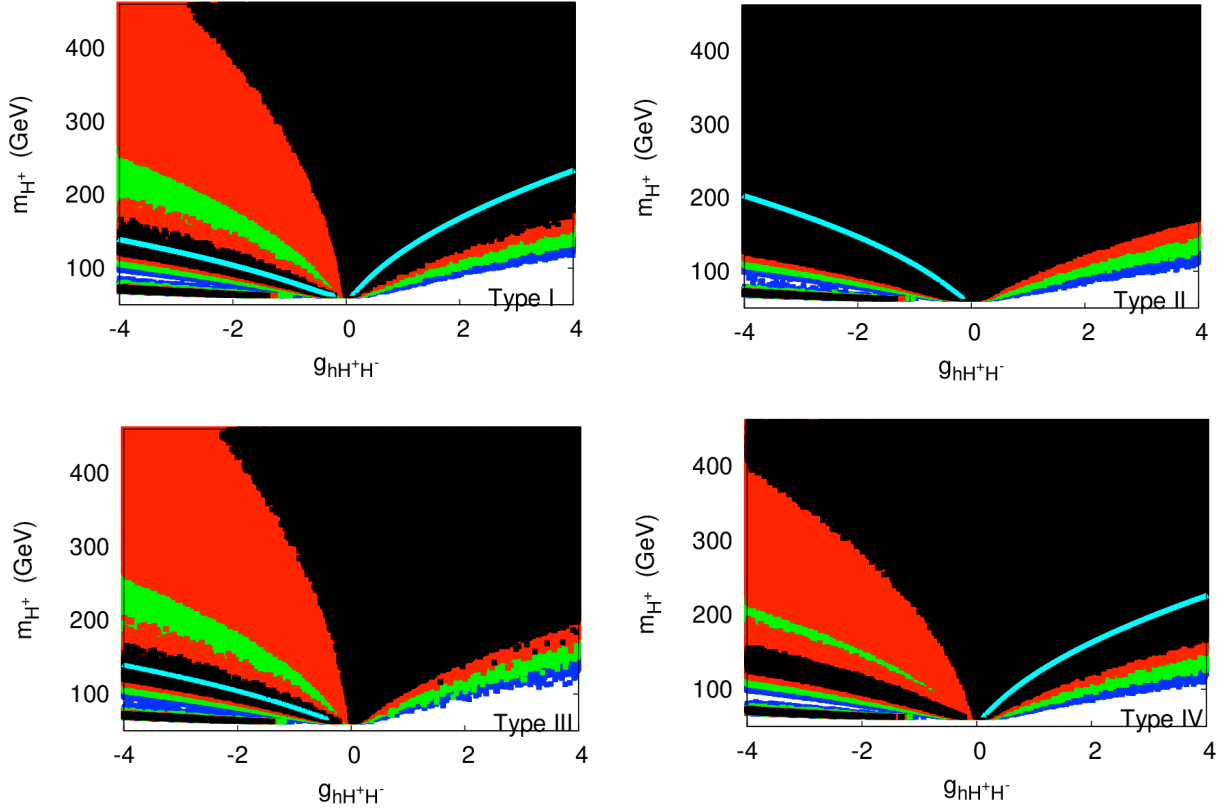


FIG. 22. The same as Fig. 16 but we used $g_{hH^+H^-}$ and m_{H^\pm} in place of $(\Delta S^\gamma)^{H^\pm}$ for Type I – IV (**CPV4**). The contour regions shown are for $\Delta\chi^2 \leq 1.0$ (black), 2.3 (red), 5.99 (green), and 11.83 (blue) above the minimum, which correspond to confidence levels of 39.3%, 68.3%, 95%, and 99.7%, respectively. The best-fit points are denoted by a beam of cyan triangles.